

Trisomy 11, 12, and 16 in *v-abl/myc*-induced murine plasmacytomagenesis

By

Marlon Luke Hagerty

A Thesis Submitted to the Faculty of Graduate Studies
In Partial Fulfillment of the Requirements of the Degree of

MASTER OF SCIENCE

Department of Physiology
University of Manitoba
Winnipeg, Manitoba

Copyright © 2007 by Marlon Luke Hagerty

TABLE OF CONTENTS

	Page
ABSTRACT	iii
ACKNOWLEDGEMENTS	v
LIST OF FIGURES	vii
LIST OF TABLES	viii
LIST OF ABBREVIATIONS	ix
1. INTRODUCTION	1
1.0 The immune system and B cell neoplasia	1
1.1 Murine plasmacytoma models	4
1.2 <i>Myc</i> -activating translocations	7
1.3 Pristane-induced formation of the oil granuloma	10
1.4 Specialized models of murine plasmacytomagenesis	11
1.5 Strain specificity	14
1.6 Focus of current study	16
2. MATERIALS AND METHODS	19
2.0 Mice	19
2.1 Plasmacytoma induction	19
2.2 ACK treatment	20
2.3 Histology	20
2.4 Lipopolysaccharide stimulation	20
2.5 Spectral karyotype analysis	21
2.6 Statistical analysis	24
3. RESULTS	26
3.0 Plasmacytoma induction in BALB/cRb6.15 mice	26
3.1 Spectral karyotype analysis	27
4. DISCUSSION	58
4.0 Effectiveness of pristane-treated mice as a control group	58
4.1 Nonrandom chromosome loss and random aneuploidy	60
4.2 Nonrandom translocation and chromosome gain	61
4.3 Additional mutations	65
4.4 Mutations in the context of other neoplasias	68
5. CONCLUSIONS	71
6. REFERENCES	72

ABSTRACT

Murine plasmacytoma is induced by plastic implants, injection of paraffin oil or pristane, or through viral infection, and *Myc* is invariably overexpressed in the tumour cells. Although translocation and juxtaposition of the *Myc* locus to an immunoglobulin locus is the prominent nonrandom cytogenetic aberration observed, the significance of other karyotypic instabilities in murine plasmacytoma is not clear, including the previously observed occurrence of trisomy 11. As well as identifying new cytogenetic mutations in murine plasmacytomagenesis, this study provides evidence for their combined and sequential accumulation that may offer new parallels to human B-cell malignancies. Plasmacytomas were induced in Balb/c Rb6.15 mice by intraperitoneal (i.p.) pristane injection prior to infection with the ABL-MYC retrovirus, and confirmed by histological examination. Spectral karyotype analysis of tumour samples identified frequent aneuploidy, tetraploidy, and amplification of chromosomes 11, 12 and 16. In contrast, control mice treated by i.p. pristane injection did not develop plasmacytoma, and lipopolysaccharide-stimulated splenocytes from control mice had mainly normal diploid karyotypes. However, karyotypic instability in a minority of splenocytes indicated that control mice showing no signs of plasmacytoma development nevertheless are prone to numerical and structural cytogenetic mutations that may possibly result in plasmacytoma initiation and progression under favourable conditions, such as infection with ABL-MYC virus with the resulting high expression of *v-abl* and *Myc* in target cells. These results indicate the possible existence of proto-oncogenes present on murine chromosomes 11, 12, and 16 that are important for plasmacytoma initiation and/or progression. There are also indications that T(1;6) and monosomy of the X chromosome

may also play roles in plasmacytomagenesis, and that trisomy 12 may only occur in cells with pre-existing nonrandom mutations, thereby acting as a late mutation event. As other experimental models of murine plasmacytoma have not shown a similar karyotypic etiology, there appears to be several possible redundant cytogenetic mutation events that lead to plasmacytoma. Also, as tumours in this study present various combinations of the aforementioned amplified chromosomes, their combined amplification may serve redundant purposes as well.

ACKNOWLEDGEMENTS

I would like to thank my supervisor, Dr. Sabine Mai, for welcoming me into the lab, both initially during my summers as an undergraduate student, and then most recently as a graduate student and her first trainee in the Canadian Institutes of Health Research programme in Innovative Technologies in Multidisciplinary Health Research Training (ITMHRT). During this period of research I have had opportunities to learn advanced laboratory techniques and meet interesting colleagues from around the world. I would like to thank all of the past and present Mai lab members for their helpful discussions, and in particular, Greg, Ted, Tony and Alice. Without Greg's extremely clear and thorough explanations of how to conduct experiments, I would not have been able to accomplish what I did.

My first undertaking as a Master's student and ITMHRT trainee was to explore an opportunity for research at Dr. Petra Boukamp's laboratory at the German Cancer Research Center in Heidelberg, Germany, during the fall and winter of the 2002-2003 academic year. This very memorable period provided a time for thought-provoking research and excellent discussion with Dr. Boukamp and the researchers at her lab. I would particularly like to thank Ana, Sharareh, Sonya, and Felix for the great time we had together.

With such a large proportion of my research focused on mouse experimentation, I would like to thank Terry Germscheid for being available to discuss my many questions on how to handle mice as effectively as possible.

Finally, I would like to thank my committee members; Dr. Angelika Dawson, Dr. Mary Lynn Duckworth, and Dr. Bob Shiu, for attending my numerous committee meetings and offering their support for my successful completion of the thesis research.

LIST OF FIGURES

	Page	
Figure 1.	Survival analysis of pristane-treated (n=7) and pristane + ABL-MYC virus-treated (n=18) BABL/cRb6.15 mice.	31
Figure 2.	Ascites smear isolated from BALB/cRb6.15 mouse treated with i.p. injection of pristane + ABL-MYC virus.	32
Figure 3.	Summary of spectral karyotype analysis of lipopolysaccharide-stimulated splenocytes originating from pristane-treated BALB/cRb6.15 mice.	33
Figure 4.	Summary of spectral karyotype analysis of ascites samples from pristane + ABL-MYC virus-injected BALB/cRb6.15 mice.	34
Figure 5.	Spectral karyotype summary of mouse C2.16.	39
Figure 6.	Spectral karyotype summary of mouse C1.15.	40
Figure 7.	Spectral karyotype summary of mouse C3.13.	41
Figure 8.	Spectral karyotype summary of mouse C5.17.	42
Figure 9.	Spectral karyotype summary of mouse C3.16.	43
Figure 10.	Spectral karyotype summary of mouse C3.17.	44
Figure 11.	Spectral karyotype summary of mouse C1.17.	45
Figure 12.	Spectral karyotype summary of mouse 3.14.	46
Figure 13.	Spectral karyotype summary of mouse 2.7.	47
Figure 14.	Spectral karyotype summary of mouse 3.15.	48
Figure 15.	Spectral karyotype summary of mouse 1.12.	50
Figure 16.	Spectral karyotype summary of mouse 2.14.	51
Figure 17.	Spectral karyotype summary of mouse 1.11.	52
Figure 18.	Spectral karyotype summary of mouse 1.13.	53
Figure 19.	Spectral karyotype summary of mouse 4.15.	54
Figure 20.	Spectral karyotype summary of mouse 4.13.	55
Figure 21.	Spectral karyotype summary of mouse 1.14.	57

LIST OF TABLES

		Page
Table I.	Solid tumours identified at necropsy.	35
Table II.	Frequent karyotypic aberrations observed in ascites tumour samples.	37
Table III.	Summary of statistically significant chromosome ploidy differences between samples of plasmacytoma tumour and control splenocytes, using the Kruskal-Wallis non-parametric test.	38

LIST OF ABBREVIATIONS

A-MuLV	Abelson murine leukemia virus
BSA	bovine serum albumin
DAPI	4'6-diamidino-2-phenylindole
FISH	fluorescent <i>in situ</i> hybridization
Ig	immunoglobulin
<i>IgH</i>	immunoglobulin heavy-chain locus
<i>Igκ</i>	immunoglobulin κ light-chain locus
<i>Igλ</i>	immunoglobulin λ light-chain locus
i.p.	intraperitoneal
H2-L ^d	L ^d gene of the major histocompatibility complex
LPS	lipopolysaccharide
MGUS	monoclonal gammopathy of undetermined significance
PKC	protein kinase C
PMA	phorbol 12-myristate 13-acetate
SCID	severe combined immunodeficiency
sIg	surface immunoglobulin
sIL-6R α	soluble IL-6 receptor α
SKY	spectral karyotype

1. INTRODUCTION

Studies focusing on the etiology of murine plasmacytoma began in the 1950s, when Merwin and Algire (1959) implanted diffusion chambers into the peritoneum of BALB/c mice and observed formation of ascites and solid tumour nodules in the peritoneum, along with metastases to spleen, lymph node, ovary, and pituitary. Since then, continued studies of murine plasmacytoma have gained relevance to human cancers such as multiple myeloma and Burkitt's lymphoma, and they have also made a broader impact in cancer research through genetic and cytogenetic inquiries that focus on predisposition to cancer (Potter, 2003). Recent investigations linking susceptibility to murine plasmacytoma with strain-specific genetic heterogeneity may also help describe the complex multifactorial nature of predisposition and incidence of both hereditary and non-hereditary human cancers (Potter, 2003; and Gado *et al*, 2001). Besides such a broad applicability in cancer research for studying murine plasmacytoma, there are also specialized areas of study where this model of carcinogenesis is relevant. Of these, topics such as the immune system and B cell neoplasia, cancer cytogenetics and tumour-specific mutations, and virus-induced carcinogenesis are discussed here as they relate to murine plasmacytoma.

1.0 The immune system and B cell neoplasia

The immune system comprises a complex collection of cells, cell signals (e.g. cytokines and chemokines) and tissues that function collectively to protect the organism against infection by mounting both an antigen-specific targeted immune response, and a more generalized response to eliminate pathogens (Janeway *et al*, 2001). To prevent or fight infection, the generalized innate immunity response relies on mechanisms that are

triggered by the presence of pathogen-associated recognition molecules such as mannose and lipopolysaccharide (LPS), and that evokes phagocytosis by macrophage and infiltrating neutrophils, complement activation, and inflammation. Along with physical barriers, such as the shedding of epithelial layers of skin and gastrointestinal lumen wall, innate immunity represents a non-specific and rapidly responding defense to possible infection. Conversely, the adaptive immune response is mediated by the activity of B- and T-lineage cells recognizing specific and unique non-self antigens, and develops “memory” of the antigen for a more rapid response upon the occurrence of reinfection.

The B and T cell development and differentiation pathways lead to genetic recombination and mutation events that allow these cells to recognize non-self antigens and mount an adaptive immune response (Janeway *et al*, 2001). B cell neoplasia encompasses many types of cancer, where cells of the B cell lineage fail to develop, maintain proper physiological function, and die according to healthy and normal biological processes (Klein, 1995). Instead, these cells proliferate to a point where histological and physiological order is lost, and tissues affected by neoplastic growth are no longer able to function adequately or properly, ending with signs of pathology. Although neoplasia—or aberrant cell division causing tumour development—of B cells occurs with many variations, there is a theme that often underlies its progression—genetic instability (Stevenson *et al*, 2001).

One example in humans is Burkitt’s lymphoma, where neoplastic B cells often carry a translocation of chromosomes 8 and 14, thereby linking the *MYC* locus with the immunoglobulin heavy-chain locus (*IgH*), respectively (Taub *et al*, 1982). Translocation can also occur between *MYC* and one of the Ig light-chain loci of chromosomes 2 (*Igκ*)

(Davis *et al*, 1984) and 22 (*Igλ*) (Hollis *et al*, 1984), also resulting in Burkitt's lymphoma, although these mutations occur less frequently. As B cells inherently express immunoglobulin, *MYC* is co-expressed due to translocation, driving cell proliferation and tumour progression. Similarly, certain forms of murine plasmacytoma were found to present analogous translocations, where immortalized plasma cells carry translocations that link *Myc* (analogous to human *MYC*) to an Ig locus, causing *Myc* overexpression (Dunnick *et al*, 1983) (discussed further in section 1.1).

Multiple myeloma also carries translocations of the Ig heavy-chain locus, where various genes may act as translocation partners (including *MYC*, although infrequently) (Seidl *et al*, 2003), and tumour cells occur as immortalized plasma cells (Shapiro-Shelef and Calame, 2004). Nowell and Hungerford (1960) identified chronic myelogenous leukemia as the first human cancer to be associated with a specific translocation: t(9;22)(q34;q11.2). The resulting hybrid gene on der(22)t(9;22), also known as the Philadelphia chromosome, is produced by a chimeric fusion of the *BCR* and *ABL1* genes, and results in a novel fusion protein with abnormal tyrosine kinase activity (Rowley, 1973). Acute lymphocytic leukemia occurs with the development of tumorigenic blast cells and has been associated with specific translocations, where t(12;21) has been detected in B cell lineage tumour cells of patients (Romana *et al*, 1994), as well as der(22)t(9;22), similar to chronic myelogenous leukemia (Hermans *et al*, 1987). In these examples, specific and characteristic genetic mutations play a key role in neoplasia. Clinical manifestation of B cell neoplasia may be evident with irregular white blood cell count, enlarged lymph nodes and spleen, hyperglobulinemia, solid tumour formation both within and outside the lymphatic system, as well as other signs. Stimulated lymphocytes

isolated from blood, and blast cells isolated from bone marrow, are less technically demanding to examine cytogenetically than cells from solid tumours, since chromosome preparations of mitotic single cell suspensions are more easily prepared for cytogenetic analysis. For this reason, many specific karyotypic mutations have been identified in leukemias, while less is known about the karyotypic mutations present in lymphomas and other solid, non-hematopoietic tumours.

As outlined in the following sections, murine plasmacytoma consistently occurs with *Myc* overexpression, with the *Myc*-activating translocation being a defining feature (Janz *et al*, 1993), while the importance of other genes and their products have also been verified, in part by cytogenetic studies (Potter, 2003). Since pristane-induced plasmacytomas—with few exceptions—carry distinct *Myc*/Ig locus translocations, these *Myc*-activating cytogenetic events are clearly necessary for the tumour to develop, and may even be initiating events (Janz *et al*, 1993). However, the identified landscaper genes *Cdkn2a* (Zhang *et al*, 1998) and *Frap* (Bliskovski *et al*, 2003), conferring genetic resistance or susceptibility to plasmacytoma, along with the effects of *Abl* (Rosenbaum *et al*, 1990) and *IL-6* (Kovalchuk *et al*, 2002) overexpression, add additional dimensions to the cause of plasmacytomagenesis. The roles of these additional genes are discussed below.

1.1 Murine plasmacytoma models

Murine plasmacytoma develops as both a solid and liquid tumour, and is the closest murine model of human multiple myeloma, in that the tumour cells of both diseases are phenotypically and genetically similar to plasma cells, where immunoglobulin heavy chain class switching has occurred and cells secrete

immunoglobulin (Potter, 2003). Although these murine and human cancers show significant similarities, it is not clear if analogous transformation events occur as well. Human multiple myeloma occurs primarily in the bone marrow, where tumour cells and bone marrow stromal cells produce and secrete TGF- β , acting as a stimulant for bone marrow stromal cells to produce the myeloma growth factor, IL-6 (Urashima *et al*, 1996). While IL-6 is also a key factor in murine plasmacytoma growth (Kovalchuk *et al*, 2002), few mouse models of plasmacytoma recapitulate the anatomical selectivity of multiple myeloma for the bone marrow, and thus the role of the bone marrow stromal cell and its associated paracrine signaling is largely absent in mouse studies. Also, while the postfollicular B-lineage cell is the target of transformation in multiple myeloma (Bakkus *et al*, 1992), this is less clear for murine plasmacytoma, since experimental results have highlighted several stages in B cell development that are linked to the oncogenic process. By comparing the human and murine diseases, it will be possible to develop both more accurate murine models for multiple myeloma, and identify improved treatment regimens and more precise targets for anticancer therapy.

There are a variety of methods used to induce murine plasmacytoma. Unlike the predominant use of pristane as a plasmacytoma-inducing agent in BALB/c mice (Potter and Wax, 1983), where the bone marrow is not affected by tumour growth, the several mouse models that do include multiple myeloma-like osteolytic bone lesions lend additional association between murine plasmacytoma and human multiple myeloma. For example, aging C57BL/KaLwRij mice show a low level (0.5%) incidence of spontaneous plasmacytoma that occurs in the bone marrow and is accompanied by osteoporosis, akin to human multiple myeloma (Radl *et al*, 1996). Primary tumours from these mice have

since been propagated by transferring tumour cells of the bone or spleen intravenously into recipient mice, and the individual tumour transplantation lines form part of the 5TMM tumour series (Vanderkerken *et al*, 2003). In a previously developed model, the *gag-abl* fusion gene [from the Abelson murine leukemia virus (A-MuLV)] was linked to the immunoglobulin heavy chain enhancer and an SV40 promoter, microinjected into fertilized mouse eggs of a C57BL/6 X SJL cross, thereby establishing the E μ -v-*abl* transgenic mouse with spontaneous plasmacytoma developing in mesenteric lymph node, peritoneum, and bone marrow (Rosenbaum *et al*, 1990). The various mouse models of plasmacytomagenesis offer different perspectives on how cancer could occur in a healthy animal, in a cell type that, enigmatically, is terminally differentiated and thus is not dividing or accumulating oncogenic mutations. As the 5TMM and E μ -v-*abl* models feature bone marrow involvement similarly to multiple myeloma, they provide a more rigorous histopathological approach for application to human biology, compared to other murine models of plasmacytomagenesis.

Explanations of murine plasmacytoma development that have been derived from the various mouse models differ and sometimes contradict each other, and several published studies on murine plasmacytoma indicate that, unlike multiple myeloma, the plasma cell may not be the target of cell transformation and tumorigenesis (Potter, 2003). At present, the identity of the progenitor cell type for murine plasmacytoma is not clear (e.g. terminally differentiated plasma cell, mature B cell, pre-B cell, or pro-B cell) as there are conflicting published results, as demonstrated by experimentation with the ABL-MYC virus. Supporting the view that the tumour progenitor may be an immature B cell, Weissinger *et al* (1993) injected ABL-MYC virus-infected immature B cells [$>99\%$

surface Ig M⁻ κ⁻ Thy-1⁻ Th-B⁻ B220^{dull+} FcR⁺ Bp-1(6C3)⁺] into recipient mice and observed plasmacytoma tumour development, with tumour cells harboring ABL-MYC virus-associated DNA. This study demonstrated the ability of immature B cells to act as the progenitor of plasmacytoma, using the most potent plasmacytoma-inducing agent developed to date. Remarkably, when use of the ABL-MYC virus was initially studied for its plasmacytomagenic effect, the rapid tumour development observed 15 days following i.p. injection of virus led the authors to conclude that mature B cells were being transformed (Largaespada *et al*, 1992). This apparent contradiction is somewhat clarified by Ohno *et al* (1999) using another transplantation approach; severe combined immunodeficiency (SCID) mice lacking functional B and T cells were reconstituted with either surface immunoglobulin⁺ (sIg) mature and immature B cells, or sIg⁻ plasma cells of BALB/c mice, and treated with i.p. injection of pristane and A-MuLV. In this experiment, mice reconstituted with B cells developed plasmacytomas, while those reconstituted with plasma cells did not. The combined results of these studies suggest that the B cell, and not the fully differentiated plasma cell, is the target of transformation, but there is insufficient evidence to identify the stage(s) of B cell development vulnerable to transformation. However, as physicochemical, transgenic, and viral approaches may offer parallel routes to plasmacytoma induction, it is possible that there is not a single stage only in B cell development that is vulnerable to plasmacytomagenesis.

1.2 Myc-activating translocations

There is a stage in B cell development at which cellular activity uniquely resembles that observed in plasmacytomagenesis. Class switch recombination occurs in antigen stimulated B cells and involves intrachromatid recombination at the constant

region of the immunoglobulin heavy chain locus by VDJ-C joining, thereby shifting the cell lineage from producing antibodies of one isotype to another (Janeway *et al*, 2001). Also, the variable regions of the immunoglobulin heavy and light chain loci undergo somatic recombination at the pro-B, pre-B, and immature B cell stages (V-D-J and V-J recombination for the heavy chain and light chains, respectively), resulting in production of a diversity of antigen specificities across the population of developing B cells (Janeway *et al*, 2001). The most frequent karyotypic mutation observed in murine plasmacytoma involves the immunoglobulin heavy chain, where *Myc* on chromosome 15 is translocated to the S_α switch region of the immunoglobulin heavy chain on chromosome 12 (Janz *et al*, 1993), producing the T(12;15) mutation, and somewhat resembling class switch recombination for production of IgA immunoglobulin. Through this reciprocal translocation, *Myc* is placed under the transcriptional control of the immunoglobulin heavy chain locus, thereby explaining how *Myc* is overexpressed in the tumour cells (Dunnick *et al*, 1983). Dysregulation of *Myc* protein levels—and in multiple myeloma, *MYC*, the human homolog—is widely observed, although for murine plasmacytoma this occurs due to transcriptional upregulation, while in multiple myeloma, it may occur either by increased transcription or translation (Paulin *et al*, 1996; Potter and Wiener, 1992; and Selvanayagam *et al*, 1988). The myelocytomatosis oncogene (reviewed by Mai and Mushinski, 2003) family has members that include *Myc*, B-*Myc*, L-*Myc*, N-*Myc*, P-*Myc*, and R-*Myc*. *Myc* is a member of the helix-loop-helix/leucine zipper protein family that binds E-box consensus sequences (CANGTG, where N=T or C) to regulate transcription upon heterodimerization with the transcription factor Max, thereby promoting transcription. However, *Myc*/Max heterodimers also bind *Inr*

elements, which form part of the promoter region of genes, leading to transcriptional repression (Gartel and Shchors, 2003). Myc is a multifunctional protein that enhances transcription of growth-promoting genes while repressing transcription of growth-arresting genes. Also, Myc overexpression may drive genomic instability and induction of apoptosis, but molecular mechanisms for these additional roles are not established (Prochownik and Li, 2007).

Generation of T(12;15) is likely an initiating step for the majority of plasmacytomas induced by i.p. injection of pristane with or without Abelson virus infection, and is detected in tissues before there is histological evidence of tumour growth (Janz *et al*, 1993). This cytogenetic mutation has been described in murine plasmacytomas since 1979 (Ohno *et al*, 1979), and has been termed the “typical” translocation, while two other “variant” translocations have also been identified that act similarly at the genetic and cellular level. While T(12;15) occurs in approximately 80% of pristane-induced murine plasmacytomas, T(6;15) is the principal mutation identified in the remaining tumours, where the constant region of the *Igκ* locus, on chromosome 6, is translocated to the first exon of the *Pvt1* locus, on chromosome 15, situated at least 72 kb downstream of *Myc* (Siwarski *et al*, 1997; Cory *et al*, 1985). Additionally, a rarely occurring and analogous translocation between the *Igλ* locus on chromosome 16 and *Pvt1* has been identified (Axelson *et al*, 1991). In both of these cases of murine plasmacytoma with the “variant” T(6;15) and T(15;16) mutations, the translocation results in overexpression of Myc (Potter and Wiener, 1992). As immunoglobulin light chain gene rearrangement occurs in pre-B and immature B cells, it is conceivable that these *Myc*-activating “variant” translocations occur in these stages of B cell development, although

this has not been shown (Potter and Wiener, 1992). This would imply that the oncogenic *Myc*-activating mutation only results in tumourigenesis once the mutated cell or its progeny gains the differentiated plasma cell-like phenotype observed in plasmacytoma, possibly induced by cell migration into the growth-stimulating peritoneal environment that occurs upon chronic inflammation in pristane-treated mice (Potter, 2003).

It is clear that activation of *Myc* is not sufficient for plasmacytoma to occur, as *Myc*/Ig translocations have been detected in secondary lymphoid organs of both BALB/c mice and various plasmacytoma-resistant mouse strains, without prior treatment of pristane (Müller *et al*, 1997). These interesting results imply a spontaneous occurrence of *Myc*/Ig translocations in healthy mice, but under these circumstances they do not lead to tumour formation. Such results suggest that there may be further steps necessary for tumourigenesis following *Myc* activation, or that the *Myc*/Ig translocation only results in *Myc* overexpression at a later stage of tumour development, effectively decoupling *Myc*/Ig translocation from *Myc* overexpression. In any case, while the contextual importance of translocation events and *Myc* overexpression is unclear, a multi-step model of carcinogenesis is applicable for describing murine plasmacytoma, especially when deregulation of *Myc* is combined with other observed pathological changes (Kovalchuk *et al*, 2003).

1.3 Pristane-induced formation of the oil granuloma

An important feature in murine plasmacytomagenesis, apart from the genetic mutations spontaneously occurring in B-lineage cells, appears to be a microenvironment hospitable for progenitor cells to grow into tumours, which develops *de novo* in the peritoneum under certain conditions (Potter and Wiener, 1992). Potter and MacCardle

(1964) found that i.p. injection of non-metabolizable oils acts as a stimulant for chronic inflammation, with macrophages surrounding oil droplets and adhering to the mesothelium of the mesentery, progressing further with continued encapsulation of the oil by mesothelium, to form numerous vascularized nodules. This tissue, termed oil granuloma, also forms in other parts of the peritoneal cavity, occurring as free-floating pedunculated bodies, or adhering to the spleen and diaphragm. The oil granuloma also contains fibroblasts, plasma cells, undifferentiated mesenchymal cells and megakaryocytes (Potter and MacCardle, 1964), thereby showing some resemblance to bone marrow. Even in mice resistant to plasmacytoma induction by pristane, the oil granuloma develops with foci of plasma cells (Potter *et al*, 1994). Unlike many carcinogens such as DNA mutagens that act due to their chemical properties, the oil granuloma develops in reaction to the physical presence of an agent that causes chronic inflammation. Similarly, in humans, a chronic immune response condition called monoclonal gammopathy of undetermined significance (MGUS) can lead to multiple myeloma (reviewed by Kyle and Rajkumar, 2003). In this way, although formation of the oil granuloma is limited to the laboratory environment, it may offer correlations with early stages of multiple myeloma. Disease progression beyond this benignity has been studied in a variety of murine models, in addition to pristane treatment in BALB/c mice.

1.4 Specialized models for studying murine plasmacytomagenesis

Many murine models more specialized than pristane induction in the susceptible BALB/cAn strain have been used to study specific aspects of plasmacytomagenesis. In this way it has been possible to clarify, or more rigorously challenge, the assumptions and conclusions drawn from previous experiments.

A prime example is the use of *Myc*-overexpressing mice in the E μ -*myc* transgenic model, where the murine *Myc* gene driven by the heavy chain enhancer E μ was microinjected into fertilized ova, whereupon the resulting mice developed a high incidence of multifocal pre-B and B cell lymphomas, but not plasmacytomas, with tumours showing high expression of the E μ -driven *Myc* gene while endogenous *Myc* expression was not detected (Adams *et al*, 1985). A similar profile for gene expression was observed in cell lines from oil-induced murine plasmacytomas, where *Myc* was expressed only from the translocated allele (Adams *et al*, 1983; Bernard *et al*, 1983). These results imply that *Myc* overexpression resulting from chromosome translocation in B-lineage cells is not sufficient for plasmacytomas to develop, and that a more complex model that is not exclusive to *Myc* overexpression is required to explain how plasmacytoma development occurs (Silva *et al*, 2003).

The role of IL-6 in plasmacytomagenesis has also been more thoroughly assessed by using IL-6 overexpressing and knockout mice. Initially, IL-6 was identified as a required growth factor for *in vitro* culture of primary plasmacytomas (Degraffi *et al*, 1993), comparable to culture of primary multiple myelomas (Kawano *et al*, 1988). While cultures of plasmacytoma cell lines T1165 and T1198 in media lacking IL-6 led to apoptosis, stimulation by phorbol 12-myristate 13-acetate (PMA) rescued these cells from apoptosis and was dependant on protein kinase C (PKC) (Romanova *et al*, 1996). Since changes in expression of various PKC isoenzymes were not correlated with PMA-mediated suppression of apoptosis in IL-6-starved plasmacytoma cell cultures, it was hypothesized that IL-6 acted as a growth factor in part by effecting changes in PKC activation, but not PKC abundance (Romanova *et al*, 1996). A study by Thabard *et al*

(2001) expanded upon this hypothesis using human multiple myeloma XG-6 cells in culture, where PMA stimulation induced PKC- δ phosphorylation at Thr-505, which is essential for PKC- δ activation, and PKC isoenzymes δ and η were activated as cells secreted soluble IL-6 receptor α (sIL-6R α). Since sIL-6R α acts as an agonist for IL-6 signaling in multiple myeloma (Barille *et al*, 2000; Gaillard *et al*, 1997), it is possible that the growth-stimulating effects of IL-6 signaling in murine plasmacytoma cells also rely on sIL-6R α , in addition to PKC activation. Using a BALB/c congenic strain carrying an *IL-6* transgene driven by the promoter of the L^d gene of the major histocompatibility complex (H2-L^d), Kovalchuk *et al* (2002) observed spontaneous plasmacytoma development in a majority of mice, where tumour cells carried the T(12;15) translocation, but in recipient nontransgenic BALB/c mice transplantation required pristane preconditioning. A more recent study of this *IL-6* transgenic strain has found that plasmacytomas may rarely develop in the absence of a *Myc/Ig* translocation, although *Myc* is still overexpressed in *trans* in these tumours (McNeil *et al*, 2005). Conversely, *IL-6* knockout mice do not develop plasmacytoma (Hilbert *et al*, 1995).

As an addition to the classical plasmacytoma induction system, A-MuLV was found to induce plasmacytomagenesis with a relatively moderate latency period (30 to 100 days) and low efficiency (up to 20%), with characteristic *Myc/Ig* translocations observed (Potter *et al*, 1973). A-MuLV contains *v-Abl*, an analogue of the *c-Abl* gene (Goff *et al*, 1980), and encodes the P160^{gag-abl} tyrosine kinase (Rosenberg *et al*, 1980). Similar to *IL-6* transgenic mice, E μ -*v-abl* transgenic mice (Rosenbaum *et al*, 1990) developed a *Myc/Ig* translocation in many, but not all tumours, as detected by Northern and Southern blots to reveal gene rearrangement, leading to the possibility of parallel

mutation pathways to plasmacytoma development. Rosenbaum *et al* (1990) also crossed E μ -v-*abl* transgenic mice with E μ -*myc* transgenic mice, and found accelerated, oligoclonal plasmacytoma development. E μ -*myc* transgenic mice have also been treated with A-MuLV to develop plasmacytoma (Sugiyama *et al*, 1990). This cooperation between *Myc* and *Abl* or *Myc* and *IL-6* indicate a role for anti-apoptotic, growth, and survival factors in plasmacytoma development, complementing the effect of high *Myc* levels.

These results correspond with experiments using the ABL-MYC virus, where *Myc* has been added to A-MuLV, using the herpes simplex virus thymidine kinase promoter to maintain high levels of transcription, and this virus is able to induce plasmacytoma with both low latency and high efficiency (Largaespada *et al*, 1992). Importantly, as infected cells express high levels of virus-encoded *Myc*, a *Myc*-activating translocation is unnecessary and is not observed. ABL-MYC virus is clearly a potent plasmacytoma-inducing agent, as pristane pretreatment is not required, and strain specificity is overcome (Largaespada *et al*, 1992). Also, immunized mice infected with ABL-MYC virus develop plasmacytoma whose tumour cells produce antigen-specific monoclonal antibodies (Weissinger *et al*, 1991), which has offered commercial potential for antibody development (Largaespada *et al*, 1996).

1.5 Strain specificity

The search for strain-specific factors conferring susceptibility to murine plasmacytoma has been a major focus, in that there has not been a complete explanation for why BALB/c and NZB strains of mice are susceptible to murine plasmacytoma following intraperitoneal (i.p.) injection of plastic implants, paraffin oil, or pristane, while

other strains remain resistant to tumour formation. With a latency of between 150 and 275 days, about 60% of BALB/c mice develop plasmacytoma by the conventional protocol of three monthly i.p. pristane injections (Potter and Wax, 1983), although it appears that in more recent years, induction has not been as effective as before, and may be the result of evolution within the strain (Potter *et al*, 1997) or maintaining mice under specific pathogen-free conditions (Byrd *et al*, 1991). The search for genetic factors influencing plasmacytomagenesis within and among mouse strains through crossing and backcrossing of susceptible and resistant strains, such as BALB/c X DBA mice, has led to the identification of two “plasmacytoma susceptibility and resistance” loci on chromosome 4, termed *Pctr1* and *Pctr2* (Potter *et al*, 1994), whose allelic variants confer susceptibility to plasmacytoma. These loci have since been identified as the already cloned genes *Cdkn2a* (Zhang *et al*, 1998) and *Frap* (Bliskovski *et al*, 2003), respectively.

For *Cdkn2a*, Balb/c mice carry two single nucleotide missense mutations (Zhang *et al*, 1998), while for *Frap*, Balb/c mice carry one such mutation (Bliskovski *et al*, 2003). *Cdkn2a* encodes two proteins produced by alternative splicing, p16^{INK4a} and p19^{ARF}, and Zhang *et al* (1998) identified p16^{INK4a} variants between plasmacytoma-susceptible BALB/c and plasmacytoma-resistant DBA/2N mice differing in primary sequence. This group also found that several different BALB/c-lineage alleles encode proteins that are less efficient than the wild type DBA/2N allele in inhibiting cyclin D/CDK4 kinase activity, which is required for G1 to S phase progression. More recent work has shown that the BALB/c promoter for *Cdkn2a* is also less efficient than that of the DBA/2 mouse strain (Zhang *et al*, 2003). Additionally, *Frap* was found to contain sequence variations between BALB/c and DBA/2 mice, and its gene product was found

to be less active in BALB/c mice (Bliskovski *et al*, 2003). The genetic variants were termed “efficiency alleles” because the variations did not cause “all-or-none” changes to protein activity, but only a decreased activity. In these studies, both genes have been implicated as tumour suppressors, as hybrid strains carrying BALB/c variants for these loci confer increased plasmacytoma susceptibility in a resistant strain background. Genes on chromosomes 1 and 5 have also been hypothesized to play a role in plasmacytoma development, although specific genes have so far not been identified (Coleman *et al*, 2000).

1.6 Focus of current study

Identification of other genes important in murine plasmacytoma has been limited by the conventional induction method of i.p. pristane injection or other agents such as plastic implants that cause chronic inflammation, since the only frequent, widely observed nonrandom cytogenetic aberration that has been identified and confirmed is translocation and juxtaposition of the *Myc* locus to an Ig locus. The studies implicating *Cdkn2a* (Zhang *et al*, 1998) and *Frap* (Bliskovski *et al*, 2003) were done by sequencing, which can be labour intensive if variations across the complete mouse genome in susceptible and resistant strains are to be considered. However, another plasmacytoma induction system using the ABL-MYC virus has been developed (Largaespada *et al*, 1992) where the characteristic *Myc*/Ig locus translocation need not be present, and in such cases other frequent and nonrandom karyotypic mutations may be identified using both standard and advanced cytogenetic techniques, thereby allowing for another approach in unraveling plasmacytomagenetics.

With the ABL-MYC virus, it has been possible to identify frequent and nonrandom karyotypic mutations that may provide a more detailed understanding of how murine plasmacytoma develops. High frequency of trisomy 11 has been identified in ABL-MYC murine plasmacytoma, and specific amplification of band 11E has been hypothesized as key to ABL-MYC-induced plasmacytomagenesis (Wiener *et al*, 1995). Mouse chromosome 11 is syntenic with regions of human chromosome 1, 2, 5, 11, 16, 17, and 22, although much of the homology is with chromosome 17, including mouse band 11E. Amplification of this region of synteny, specifically, mouse chromosome 11 and human chromosome 17q, has already been characterized in several cancers, including human and murine neuroblastoma where the regions are amplified at human 17q23.1 to 17qter and murine band 11E (Lastowska *et al*, 2004), gastric cancer (Varis *et al*, 2002), and breast cancer (Coene *et al*, 1997). Conversely, deletion of this region has also been found in human cancers, such as that of lung (Fong *et al*, 1995), prostate (Gao *et al*, 1995), breast and ovary (Saito *et al*, 1993). A gene regulating tumour development in this region of synteny has so far not been clearly identified.

This research project continues the genetic analysis of ABL-MYC-induced murine plasmacytoma, with specific attention paid to chromosome 11. As the ABL-MYC virus is a potent plasmacytoma induction agent, it is important to follow karyotypic evolution with assurance of tumour clonality, where polyclonal tumour cell populations originating from different transformation events are recognized, if present, and distinguished from karyotypic evolution of monoclonal tumours where a tumour cell population originates from a single transformation event. Establishing a cytogenetic profile of ABL-MYC virus-induced murine plasmacytomas in this study allows for

comparison of these tumours with other previously characterized induction protocols, which have linked relatively few karyotypic mutations to tumour development in addition to *MYC*/Ig translocation. This study aims to identify new cytogenetic markers for murine plasmacytoma that have not been observed, either due to their low frequency in comparison to the *MYC*/Ig translocations in pristane-treated Balb/c mice, or because analyses of tumours from various induction methods have often not included extensive cytogenetic data. In this way, it becomes more feasible to construct a model for karyotypic mutation and evolution leading to murine plasmacytoma, aiding in the further identification of the amplified and overexpressed genes vital to plasmacytoma initiation and progression, while also offering new parallels to human B-cell malignancy.

2. MATERIALS AND METHODS

2.0 Mice

BALB/cAKR-Rb6.15 mice carrying a Robertsonian fusion of chromosomes 6 and 15, hereafter referred to as BALB/cRb6.15 mice, were obtained from Dr. Shinsuke Ohno (Kanazawa University, Japan) and maintained by University of Manitoba Central Animal Care Services under specific pathogen-free conditions. Mice were named according to treatment; those with names beginning with “C” were not treated with ABL-MYC virus.

2.1 Plasmacytoma induction

Female BALB/cRb6.15 mice of seven weeks of age were treated with a single i.p. injection of 0.3 ml pristane (2,6,10,14-tetramethylpentadecane) (Sigma, Canada) using a 27 ½-gauge needle. At seven weeks and five days of age, experimental group mice were additionally treated with a single i.p. injection of 0.5 ml ABL-MYC virus ($1 \times 10^3 - 1 \times 10^5$ ffu) (NeoClone, USA) using a 27 ½-gauge needle. Mice were monitored for signs of ascites formation (such as an enlarged abdomen) as well as signs of distress, including decreased mobility, difficulty with walking, abnormal breathing, spiked fur, and loss of skin elasticity. Ascites were removed between approximately 1800 h and 2000 h for each mouse, thereby minimizing sample variation (of RNA) due to circadian rhythms (Lowrey and Takahashi, 2004), via i.p. tap using a 21 ½-gauge needle, and collected into a 15 ml Falcon tube kept in ice. Mice were maintained until presenting signs of distress or until a second ascites tap was performed, whereupon euthanization was performed by carbon dioxide asphyxiation. In cases where mice did not develop ascites or present signs of distress, mice were maintained for a minimum of 14 months following pristane injection.

Euthanized mice were necropsied, and solid tumours were removed and collected into 15 ml Falcon tubes containing ice-cold RPMI medium.

2.2 ACK treatment

Mouse ascites was centrifuged at 200xg for 5 minutes, and the cell pellet was treated with 5 ml ice-cold ACK (155 mM NH₄Cl, 10 mM KHCO₃, and 137 μM EDTA, pH 7.4) for 5 minutes to lyse erythrocytes, and centrifuged at 200xg for 5 minutes. At this point, if erythrocytes were still visible in the cell pellet, another ACK treatment was performed. The cell pellet was then resuspended in ice-cold 5 ml RPMI medium, centrifuged at 200xg for 5 minutes, resuspended in 10 ml ice-cold RPMI medium, upon which cells were counted using a hemocytometer to determine cell concentration.

2.3 Histology

Ascites was spread onto slides and air-dried. Alternatively, approximately 1.5X10⁵ cells from ascites samples treated with ACK (see above) were distributed onto glass slides (Type K102, Kindler GmbH & Co., Germany) by cytopspin (1200 rpm, 5 minutes), and then air-dried. Air-dried cells on slides were fixed with methanol (Sigma, USA) for 10 minutes, stained with histological Giemsa stain (Sigma, USA) for 20 minutes, rinsed with water, and examined under oil immersion using a 100X objective, Zeiss Axioskop microscope 2, and a Polaroid DMC-3 CCD camera and Polaroid DMC 2 software (Polaroid, Canada) for analysis.

2.4 Lipopolysaccharide stimulation

Female BALB/cRb6.15 mice of seven weeks of age were treated with a single i.p. injection of 0.3 ml pristane using a 27 ½-gauge needle. Mice were euthanized by

carbon dioxide asphyxiation, dissected, and spleens were transferred into ice-cold RPMI medium supplemented with 10% heat inactivated fetal bovine serum, 1% L-glutamine, 1% sodium pyruvate, 1% penicillin/streptomycin, and 0.1% beta-mercaptoethanol (all reagents GIBCO BRL, Canada). Using a 27 ½-gauge needle, each spleen was pierced over its entire surface approximately 20 times, and using a 27 ½-gauge needle and 10 ml syringe, RPMI medium was injected into the spleen to flush out splenocytes. Splenocytes were incubated for 30 minutes in 15 ml cultures of RPMI medium in Nuclon™Δ 100 mm diameter polystyrene tissue culture dishes (Nunc, Denmark) at 37°C, 5% CO₂ to allow binding of adherent cells, whereupon non-adherent splenocytes were transferred to fresh cultures of 1X10⁷ cells per dish, containing 10 ml RPMI medium supplemented with 20 µg/ml LPS from *Escherichia coli* serotype 0111:B4 (Sigma, Canada). Splenocytes were stimulated to divide in the presence of 20 µg/ml LPS for approximately 48 to 72 h, at which point they formed aggregates at high frequencies.

2.5 Spectral karyotype analysis

Spectral karyotype (SKY) analysis was done as described in Fest *et al* (2002). Approximately 2X10⁷ cells treated with ACK (see above), were centrifuged at 200xg for 5 minutes, resuspended and hypotonized in 0.075 M KCl for 30 minutes at room temperature, centrifuged at 129xg for 10 minutes, with the supernatant then being removed. The hypotonized cells were fixed with fresh 3:1 methanol:acetic acid by drop fixation, where fixation solution was added drop by drop by the following schedule: 5 X 1 drop with 1 minute wait following each drop; and 2, 5, 7, 10, 15, 20, 30, and 60 drops with 2 minutes wait following each round of drops. The cell pellet was resuspended by micropipetting, incubated for 10 minutes at room temperature, and centrifuged at 129xg

for 10 minutes. Cells were resuspended in 5 ml fixative, incubated for 20 minutes, and centrifuged at 129xg for 10 minutes. This last step was repeated again with a 30-minute incubation. Fixed cells were resuspended in 5 ml fixative and stored at -20°C .

To prepare metaphase spreads, using a 9 inch Pasteur pipette (Fisher, Canada), fixed cells (in 15 cm Falcon tubes) were suspended in fixative, then dropped onto glass microscope slides (Type K102, Kindler GmbH & Co., Germany) chilled on dry ice for approximately 1 minute, held approximately 1 m below the Pasteur pipette at an inclination of 45° , with approximately 2 to 3 drops of fixed cells being applied to the slides. Slides were immediately warmed on a 37°C hot plate for 3 seconds, then submerged into 50% acetic acid for 1 second, and dried on a 37°C hot plate. To evaluate slide and metaphase plate quality, dried slides were incubated for 90 seconds in 10% Giemsa solution diluted in 0.15 M $\text{K}_2\text{HPO}_4/\text{KH}_2\text{PO}_4$ phosphate buffer (pH 8.0), rinsed under tap water, air-dried, then viewed with a light microscope. Slides with high quality metaphase spreads bearing few overlapping chromosomes were aged for 2 days at room temperature.

Aged slides were equilibrated for 2 minutes in 70% ethanol (Fluka, USA), then in 2X SSC for 10 minutes. RNase A (100 $\mu\text{g}/\text{ml}$ in 2X SSC) was added to slides (100 μl per slide), and a coverslip (24X60 mm) was applied before incubating slides for 1 hour at 37°C . Slides were then washed on a shaker 3 X 5 minutes in 2X SSC, and treated with 40 $\mu\text{g}/\text{ml}$ pepsin while incubating in 0.01 M HCl for 10 minutes. Following pepsin treatment, slides were washed 2 X 5 minutes in PBS and for 5 minutes in PBS/50 mM MgCl_2 , incubated for 10 minutes in freshly prepared 1% formaldehyde/PBS/50 mM MgCl_2 , and then washed for 5 minutes in PBS. Slides were dehydrated for 3 minutes

each in 70%, 90%, and then 100% ethanol (Fluka, USA), and air-dried for approximately 5 minutes. Dry slides were incubated in an oven for 5 minutes at 70°C, transferred immediately into a 70°C denaturing solution of 70% formamide/2XSSC (pH 7.0) and incubated for 2 minutes. Denatured slides were dehydrated for 3 minutes each by transferring subquentially into chilled (-20°C) 70%, 90%, then 100% ethanol (Fluka, USA), and air-dried for approximately 5 minutes. Approximately 8-10 µl of mouse SKYPaint™ (Applied Spectral Imaging, USA), previously denatured for 5 minutes at 85°C and incubated for 1 hour at 37°C, was added to each air-dried slide, and a coverslip (25X25 mm) and rubber cement were applied to seal the SKYPaint™. Slides were then incubated for approximately 36 hours in a humidified chamber at 37°C, 5% CO₂. Following hybridization for approximately 36 hours, coverslips and rubber cement were removed, and slides were washed 3 X 5 minutes in 50% formamide/2X SSC at 45°C, then 2 X 5 minutes in 1X SSC at 45°C. One percent bovine serum albumin (BSA) (Sigma, Canada) was added to slides (80 µl per slide) as a blocking reagent, and a coverslip (24X60 mm) (Kindler GmbH & Co., Germany) was applied before incubating slides for 1 hour at 37°C. Mouse anti-digoxin (IgG, D8156, Sigma, Canada) stock (1 mg/ml) was diluted 100X in 1% BSA and added to slides (80 µl per slide, with 24X60 mm coverslip) for detection of digoxigenin-labelled DNA, before incubating slides for 45 minutes at 37°C. Slides were then washed 3 X 5 minutes in 4X SSC/0.1% Tween20 at 45°C. A mixture containing goat anti-mouse IgG (detecting mouse anti-digoxin) labeled with Cy5.5 (610-113-121, Rockland, USA), and avidin (detecting biotin-labelled DNA) labeled with Cy5 (S000-06, Rockland, USA), was prepared by diluting both stocks (1 mg/ml) 200X in 1% BSA, and was then added to slides (80 µl per slide, with 24X60 mm

coverslip). After incubating slides for 45 minutes at 37°C, slides were washed 3 X 5 minutes in 4X SSC/0.1% Tween20 at 45°C. 4'6-diamidino-2-phenylindole (DAPI)/antiblead (Applied Spectral Imaging, USA) was added to slides (one drop per slide) to counterstain DNA and minimize photobleaching.

Slides were then imaged under oil immersion at 630X magnification using a Zeiss Axioplan 2 microscope equipped with a SpectraCube SD-300 (Applied Spectral Imaging, Israel) and VDS COOL-1200QS CCD camera (VDS Vosskühler GmbH, Germany), using a PC with Spectral Imaging 4.0 software (Applied Spectral Imaging, Israel). Karyotype analysis was done using a PC with SkyView 2.1 software (Applied Spectral Imaging, Israel). Between 20 and 39 cells were analyzed for each mouse.

2.6 Statistical analysis

To identify variation in survival between mice treated with and without ABL-MYC virus, Kaplan-Meier analysis was performed using MedCalc version 8. Also, the Kruskal-Wallis non-parametric test was performed by Dr. Mary Cheang (Department of Community Health Sciences, University of Manitoba) to compare tumour samples and LPS-induced splenocyte samples in various aspects, including: (1) the occurrence of chromosome ploidy changes (chromosome gain or chromosome loss), (2) the proportion of diploid (or near diploid) cells, (3) the proportion of tetraploid (or near tetraploid) cells, (4) the proportion of cells without any detectable mutations, (5) the average number of chromosomes per cell, and (6) the number of total cells analyzed. Spearman correlation analysis was also performed by Dr. Mary Cheang to detect linkage between different cytogenetic mutations, as well as to identify sample bias, if present. Nonrandom

mutations were recognized as those being statistically significant, with p-values less than or equal to 0.0100.

3. RESULTS

3.0 Plasmacytoma induction in BALB/cRb6.15 mice

In this study, treatment with ABL-MYC virus in addition to pristane clearly enhanced ascites production and development of plasmacytoma, while accelerating the onset of mice showing signs of distress. Kaplan-Meier survival analysis of BALB/cRb6.15 mice treated with pristane, or pristane + ABL-MYC virus, is shown in Figure 1. The median time from pristane injection to death occurred at 460 days for pristane-treated mice (black solid line), but only 55 days for pristane + ABL-MYC virus-treated mice (red dotted line). Five of seven mice treated only with pristane were euthanized at old age showing no signs of distress, while the remaining two mice were euthanized at old age upon presentation of prolapsed cervix possibly due to old age (Dr. Valerie Smid, personal communication) in one mouse, and tumour growth at the left axillary region in the other mouse. In the mice treated additionally with ABL-MYC virus, death either occurred unaided (in five of 18 mice), or by euthanasia following signs of distress (in two of 18 mice) or directly after collection of a second ascites harvest (in 11 of 18 mice). A comparison between survival and pathology is presented in Table I.

Ascites production occurred in all ABL-MYC virus-treated mice (Figure 2), where, upon centrifugation, the cellular fraction regularly comprised approximately one tenth to one half of the total volume of recovered ascites. Hemorrhagic ascites was produced in four of the 18 mice treated with ABL-MYC virus, while a minor amount of blood was present in some of the remaining samples, possibly due to rupture of a blood vessel in the skin upon needle insertion. The observation of hemorrhagic ascites has been reported previously (Potter and MacCardle, 1964). Histological examination of ascites

smears indicated the presence of high quantities of plasmacytoma cells, neutrophils, and macrophages, as well as less frequently observed lymphocytes. Hemorrhagic ascites also contained numerous erythrocytes (outnumbering other cells), while the remaining samples contained few to no erythrocytes. No other cell types were found, although samples isolated from different mice showed variations in plasmacytoma cell morphology, ranging from less mature plasmablastic, to mature plasmacytic forms (Kovalchuk *et al*, 2002). Plasmacytoma cells occurred individually or as aggregates in all ascites samples.

Mice treated only with pristane did not develop ascites. The failure of this group to develop ascites was interpreted synonymously as a failure to develop plasmacytoma. However, upon necropsy, solid tumours were found in several pristane-treated mice (Table I). As these mice were old at time of euthanization (ranging from 482 to 523 days), it is not clear whether they developed tumours due to pristane treatment or simply because of old age (Dr. Valerie Smid, personal communication; Anisimov, 2003).

3.1 Spectral karyotype analysis

A detailed summary of the cytogenetic analysis done for each mouse is given in Figures 5 through 21. Figure 3 summarizes SKY analysis of LPS-stimulated splenocytes from control pristane-treated mice, showing a background of aneuploidy mostly occurring as chromosome loss. However, gain of the Robertsonian fusion chromosome, a product of centric fusion of chromosomes 6 and 15 that acts as a cytogenetic marker for the mouse strain of this study, and hereafter referred as Rb(6.15), was detected in six of seven mice, with one mouse (C1.17) containing a majority of analyzed cells with trisomy Rb(6.15). In this study, ploidy analysis for the Rb(6.15) chromosome was presented as if

gains or losses occurred in individual chromosomes 6 and 15, in order to facilitate future comparison with other studies where the fusion chromosome is not present.

Figure 4 summarizes SKY analysis of ascites samples from pristane + ABL-MYC virus-infected mice. It is important to note that tumour samples do not show complete homogeneity in observed mutations, and there appears to be distinct clones and subclones within tumour cell populations (Table II), where a “primary” karyotypic aberration underlies most cells, while “secondary” and “tertiary” events occur in subpopulations of cells. In this way, karyotypic changes were assessed in a context of stepwise accumulation of chromosome gain, loss, or other nonrandom aberrations, such as translocations or tetraploidy. For example, if all cells of a tumour sample displayed gain of a certain chromosome, it would be interpreted as a tumour-initiating mutation and a primary event. Likewise, if a subset of these cells also carried a gain of another chromosome, it would be interpreted as having occurred after the development of the primary event, and thus would be termed a secondary event. Similarly, a tertiary event was classified as a karyotypic aberration present in a subpopulation of cells containing a secondary karyotypic aberration. Interpretation of karyotypes in this way allowed comparison both within and among tumour samples, using an analysis focussed on determining chronological associations of specific karyotypic aberrations. Applying a hierarchical organization of the data was possible for all tumour samples except that from mouse 4.15, where a primary cytogenetic mutation could not be determined because both nonrandom karyotypic aberrations, trisomy 11 and trisomy 16, occurred separately in similar frequencies, as well as in combination. Multiple nonrandom cytogenetic

mutations were present in all tumour samples, with the exception of that from mouse 3.14, solely containing trisomy 11.

In all ABL-MYC virus-infected mice except 1.11, 4.15, and 4.13, trisomy 11 was observed as a primary karyotypic mutation (Table II). Trisomy 16 was the primary mutation of mouse 1.11, while secondary mutations included monosomy X, and trisomies 6 and 11. Analysis of mouse 4.15 did not resolve distinct clones within the tumour sample, as the occurrence of specific mutations could not be arranged in a hierarchy in relation to others. Mouse 4.13 was unique in that it contained only a small minority of cells with trisomy 11 (two of 27), and therefore it is unclear if the trisomy 11 mutation was tumour-specific in this mouse. Instead of trisomy 11, it appears that there were two separate tumour cell lineages in mouse 4.13, where the primary karyotypic mutation in one clonal lineage was trisomy 16, while the other lineage contained a T(1;6) translocation-bearing chromosome. The occurrence of T(1;6) was detected in two mice (4.15, 4.13), and in both instances, this mutation was found with trisomy 12. While other translocations were identified, none occurred with a frequency similar to T(1;6) suggesting a nonrandom occurrence.

Tumour samples were dominated with mutations of trisomies 11, 12, and 16, and each of these were found to be statistically significant, either alone or in all possible combinations, in comparison to LPS-stimulated splenocytes originating from pristane-treated mice (Table III). Tumour samples also contained a statistically significant higher proportion of cells with a tetraploid (or near tetraploid) complement of chromosomes, as well as loss of chromosomes 7 and X. None of these mutations (trisomies 11, 12, and 16; monosomy 7 and X; and tetraploidy) were observed in the analyzed splenocytes of

pristane-treated mice, except one instance of trisomy 16 in a sample derived from mouse C1.15 (cell S4 1-17).

Conversely, splenocytes from the pristane-treated mice contained an increased proportion of cells carrying no cytogenetic mutations ($p=0.0006$). While tumour samples from several mice contained diploid cells without any observed cytogenetic mutations, aneuploidy was overwhelmingly dominant. Apart from chromosome X, loss of chromosomes in both tumour and splenocyte samples appeared random, with the exception of mouse 1.14, with loss of chromosome 8 occurring in the majority of analyzed cells and in conjunction with other mutations.

Although chromosome loss appeared to occur randomly in the LPS-stimulated splenocytes originating from pristane-treated mice, trisomy of the Rb(6.15) chromosome was clearly not random, as it was detected in splenocytes from six of the seven pristane-treated mice. This occurred most prominently in splenocytes from mouse C1.17, with a majority of cells containing the mutation. However, since trisomy Rb(6.15) was also found in several tumour samples from ABL-MYC virus-treated mice, a difference in frequency between these groups was not statistically significant.

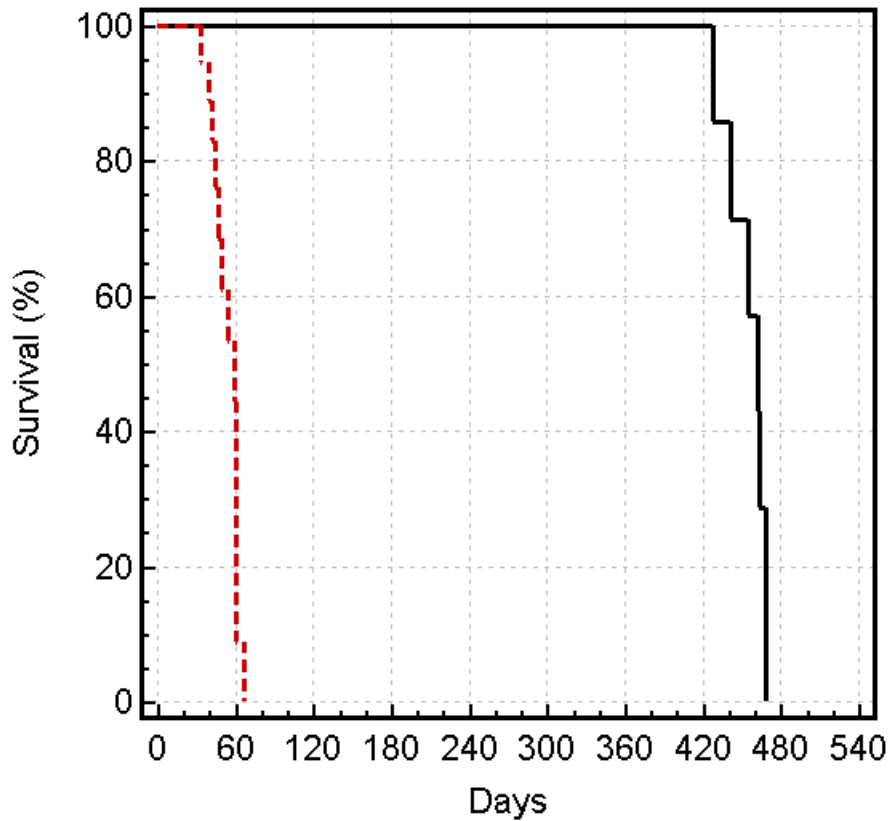


Figure 1. Survival analysis of BALB/cRb6.15 mice. Seven week-old mice were given either a 0.3 ml i.p. injection of pristane at Day 0 (n=7, black solid line), or 0.3 ml i.p. injection of pristane at Day 0 combined with an additional i.p. injection of 0.5 ml ABL-MYC virus, performed at day 5 (n=18, red dotted line). Five pristane + ABL-MYC virus-treated mice were found dead in cage, while remaining mice were euthanized. Five of seven pristane-treated mice were euthanized while displaying a healthy disposition, while all other mice (with and without ABL-MYC virus treatment) were euthanized upon presentation of signs of distress or after undergoing a second, terminal ascites harvest.

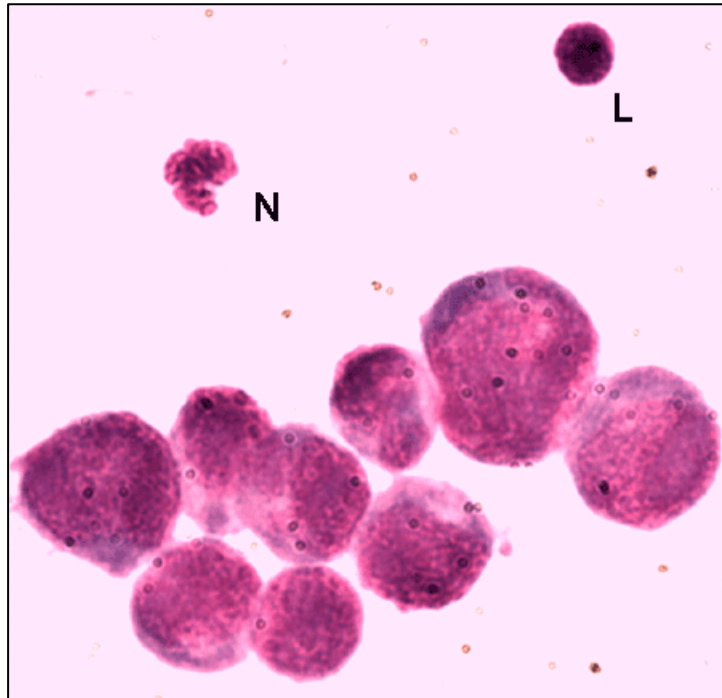


Figure 2. Ascites smear isolated from BALB/cRb6.15 mouse treated with i.p. injection of pristane + ABL-MYC virus. Cells in the lower field typify the plasmacytoma tumour cell, with a large round eccentric nucleus. N, neutrophil; L, lymphocyte. 1000x magnification.

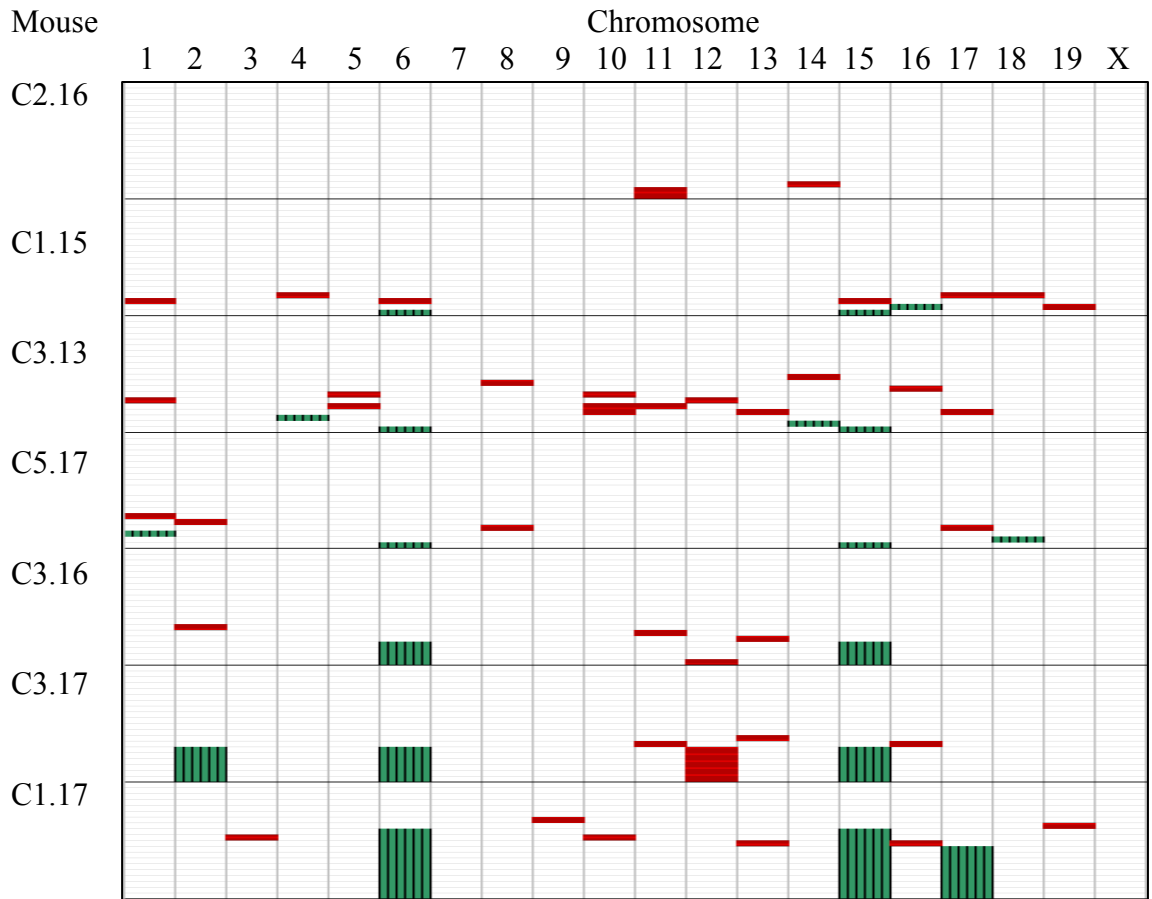


Figure 3. Summary of spectral karyotype analysis of LPS-stimulated splenocytes originating from pristane-treated BALB/cRb6.15 mice, where green stripes represent chromosome gain (trisomy or polysomy), and red stripes represent chromosome loss (monosomy or nullisomy) from metaphase plates. Metaphase plates are grouped in rows according to mouse of origin. This figure abridges data from Figures 5 through 11.

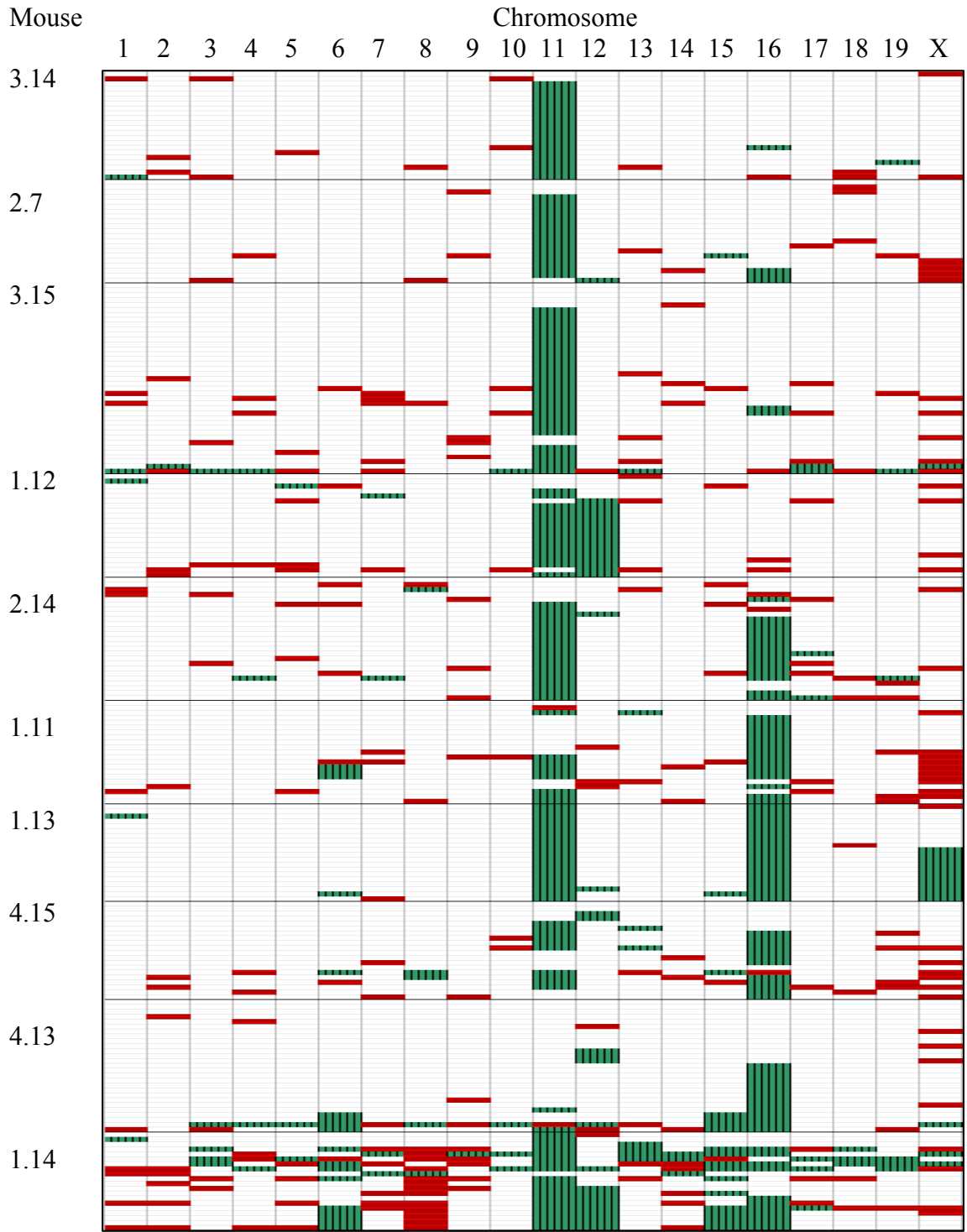


Figure 4. Summary of spectral karyotype analysis of ascites samples from pristane + ABL-MYC virus-treated BALB/cRb6.15 mice, where green stripes represent chromosome gain (trisomy or polysomy), and red stripes represent chromosome loss (monosomy or nullisomy) from metaphase plates. Metaphase plates are grouped in rows according to mouse of origin. This figure abridges data from Appendices 12 through 21.

Table I. Solid tumours identified at necropsy.

Mouse	Survival ^a	Solid Tumour Location	Ascites Recovered ^b	Karyotype Determined
C2.16	441	left axillary region	none	yes
C1.15	462	right fallopian tube	none	yes
C3.13	428	none	none	yes
C5.17	455	none ^c	none	yes
C3.16	463	none	none	yes
C3.17	468	none	none	yes
C1.17	469	none	none	yes
3.14	67	mesentery, left and right inguinal regions, numerous (~20) throughout peritoneum	6.5 ml (1) 4.0 ml (2)	yes
2.7	39	mesentery	3.5 ml 2.75 ml	yes
3.15	60	mesentery, left and right inguinal regions, posterior to spleen	5.5 ml 3.5 ml	yes
1.12	47	mesentery	3.5 ml 0.7 ml	yes
2.14	59	mesentery, inguinal region	1 ml	yes
1.11	60	mesentery, right inguinal region, posterior to spleen (six)	3.5 ml (1) 1.5 ml (2) hemorrhagic	yes
1.13	42 ^d	not determined ^e	6.0 ml (1)	yes
4.15	60	mesentery, stomach	4 drops (1)	yes
4.13	56 ^d	not determined ^e	10.0 ml (1)	yes
1.14	49	Mesentery	6.5 ml (1) 6.5 ml (2) hemorrhagic	yes
2.8	46 ^d	not determined ^e	1.0 ml (1) hemorrhagic	no
1.10	44	Mesentery	2.0 ml (1) 1.8 ml (2) hemorrhagic	no
2.11	33	Mesentery	0.4 ml (1)	no
3.11	60		0.5 ml (1) 0.5 ml (2)	no
2.12	43 ^d	not determined ^e	0.3 ml (1)	no
2.13	40 ^d	not determined ^e	none ^f	no
2.15	42	None	1.0 ml (1)	no

(a) days from i.p. injection of 0.3 ml pristane to time of death

(b) where (1) and (2) indicate volume recovered during first and second harvest, respectively

(c) mouse was euthanized upon discovery of prolapsed cervix

- (d) found dead in cage
- (e) no necropsy performed
- (f) ascites developed but was not recovered

Table II. Frequent karyotypic aberrations observed in ascites tumour samples.

Mouse	Primary Event(s)	Secondary Event(s)	Tertiary Event(s)
3.14	+11		
2.7	+11	-X, +16	
3.15	+11	<i>Subclone 1:</i> T(11;19) <i>Subclone 2:</i> Tetraploidy	
1.12	+11, +12	Tetraploidy	
2.14	+11, +16	Tetraploidy	
1.11	+16	-X, +11, +6	Tetraploidy
1.13	+11, +16	+X	Tetraploidy
4.15	not determined ^a		
4.13	<i>Clone 1:</i> T(1;6) <i>Clone 2:</i> +16	+12 +Rb(6.15)	Tetraploidy
1.14	+11	<i>Subclone 1:</i> +16, +Rb(6.15), ^b <i>Subclone 2:</i> Tetraploidy	+12, +16, +Rb(6.15), ^b

(a) Not determined due to complex hierarchical organization of cytogenetic mutations.

(b) plus other additional mutations

Table III. Summary of statistically significant chromosome ploidy differences between samples of plasmacytoma tumour and control splenocytes, using the Kruskal-Wallis non-parametric test.

Observation in plasmacytoma tumour	Significance (p-value) ^a
Loss of chromosome 7	0.0074
Loss of chromosome X	0.0004
Gain of chromosome 11	0.0004
Gain of chromosome 12	0.0074
Gain of chromosome 16	0.0024
Gain of chromosomes 11 and 12 together	0.0004
Gain of chromosomes 11 and 16 together	0.0005
Gain of chromosomes 12 and 16 together	0.0007
Gain of chromosomes 11, 12, and 16 together	0.0005
Increased proportion of near-tetraploid cells	0.0030
Decreased proportion of cells with no mutations	0.0006

(a) Statistical significance was identified with p-values less than or equal to 0.0100.

a) Summary of aneuploidy in near-diploid cells

Cell ID	1	2	3	4	5	6	7	8	9	10	11	12	13	14	15	16	17	18	19	X	None	Ch #	Notes		
S38-01																					X		40		
S38-03																						X		40	
S38-04																						X		40	
S38-13																						X		40	
S38-15																						X		40	
S38-16																						X		40	
S39-04																						X		40	
S39-06																						X		40	
S39-08																						X		40	
S39-10																						X		40	
S39-11																						X		40	
S43-03																						X		40	
S43-04																						X		40	
S43-06																						X		40	
S43-07																						X		40	
S43-08																						X		40	
S38-11																						X		40	T(12;14)
S38-06, 07, 08, 09																								39	
S39-09																								39	
S43-01, 02																								39	

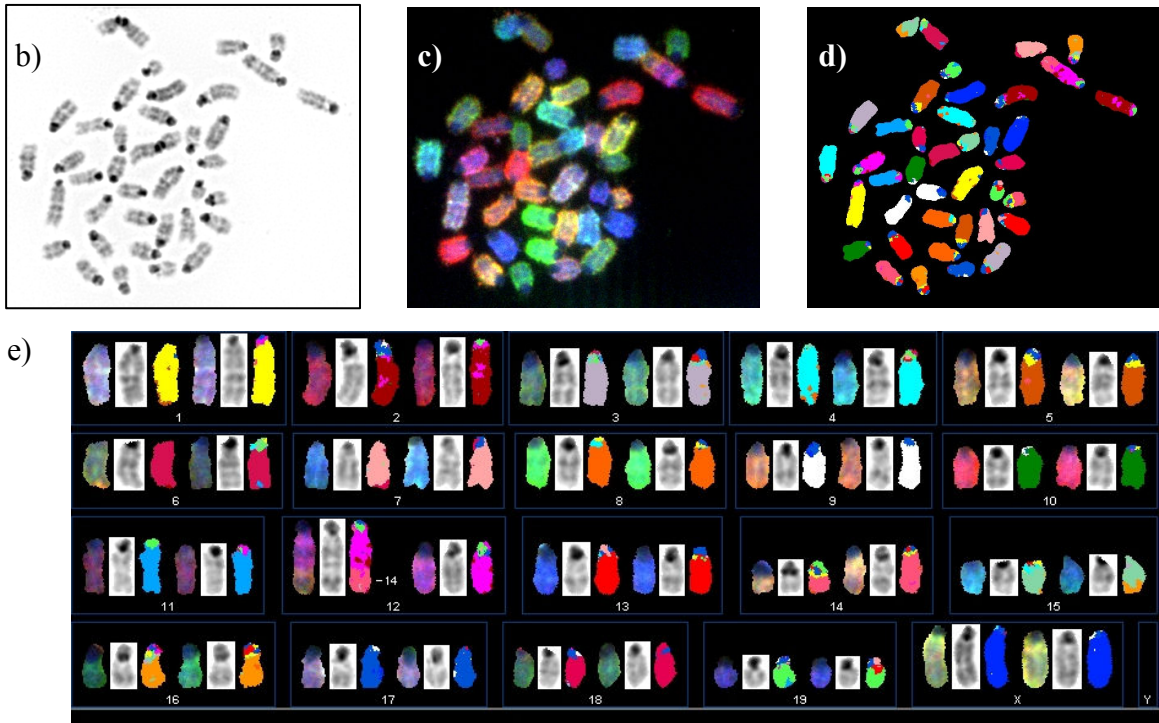


Figure 5. Spectral karyotype summary of mouse C2.16. Part a) schematically depicts karyotypes of LPS-induced splenocytes, where green blocks represent chromosome gain (trisomy or polysomy), and red blocks represent chromosome loss (monosomy or nullisomy). “None,” no aneuploidy; “Ch #,” number of chromosomes present in metaphase plate. Parts b), c), d), and e) represent inverted DAPI, spectral, classified, and karyotyped images of cell S38-11, respectively.

a) Summary of aneuploidy in near-diploid cells

Cell ID	1	2	3	4	5	6	7	8	9	10	11	12	13	14	15	16	17	18	19	X	None	Ch #	Notes		
S41.01																					X		40		
S41.02																						X		40	
S41.03																						X		40	
S41.06																						X		40	
S41.08																						X		40	
S41.10																						X		40	
S41.11																						X		40	
S41.12																						X		40	
S41.15																						X		40	
S41.16																						X		40	
S41.20																						X		40	
S41.21																						X		40	
S41.22																						X		40	
S41.24																						X		40	
S41.25																						X		40	
S41.26																						X		40	
S41.07				■													■	■	■					37	
S41.19	■								■							■								37	
S41.17															■	■						■		40	
S41.09						■	■								■	■								42	

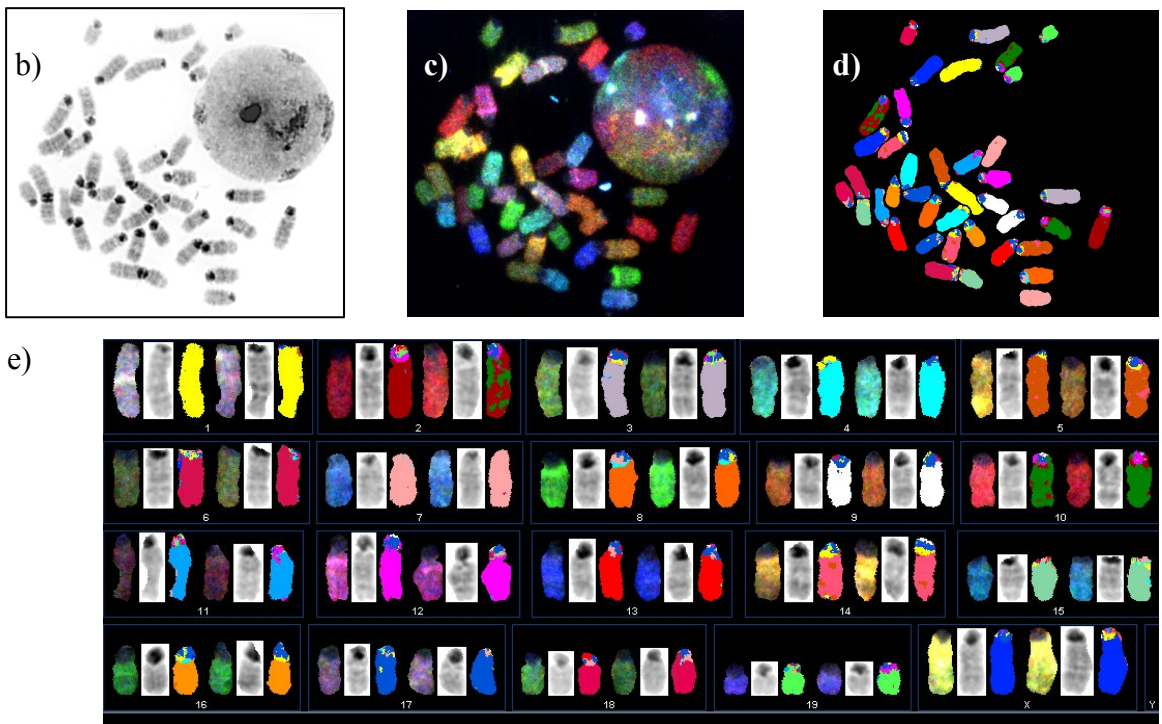


Figure 6. Spectral karyotype summary of mouse C1.15. Part a) schematically depicts karyotypes of LPS-induced splenocytes, where green blocks represent chromosome gain (trisomy or polysomy), and red blocks represent chromosome loss (monosomy or nullisomy). “None,” no aneuploidy; “Ch #,” number of chromosomes present in metaphase plate. Parts b), c), d), and e) represent inverted DAPI, spectral, classified, and karyotyped images of cell S41-22, respectively.

a) Summary of aneuploidy in near-diploid cells

Cell ID	1	2	3	4	5	6	7	8	9	10	11	12	13	14	15	16	17	18	19	X	None	Ch #	Notes	
S35-04																					X	40		
S35-06																					X	40		
S36-01																					X	40		
S36-09																					X	40		
S36-14																					X	40		
S37-05																					X	40		
S37-06																					X	40		
S37-08																					X	40		
S37-10																					X	40		
S37-14																					X	40		
S36-21																							39	
S37-16																							39	
S37-22																							39	
S36-02																							38	
S36-13																							38	
S36-06																							37	
S37-19																							37	
S35-08																							41	
S36-10																							41	
S35-02																							42	

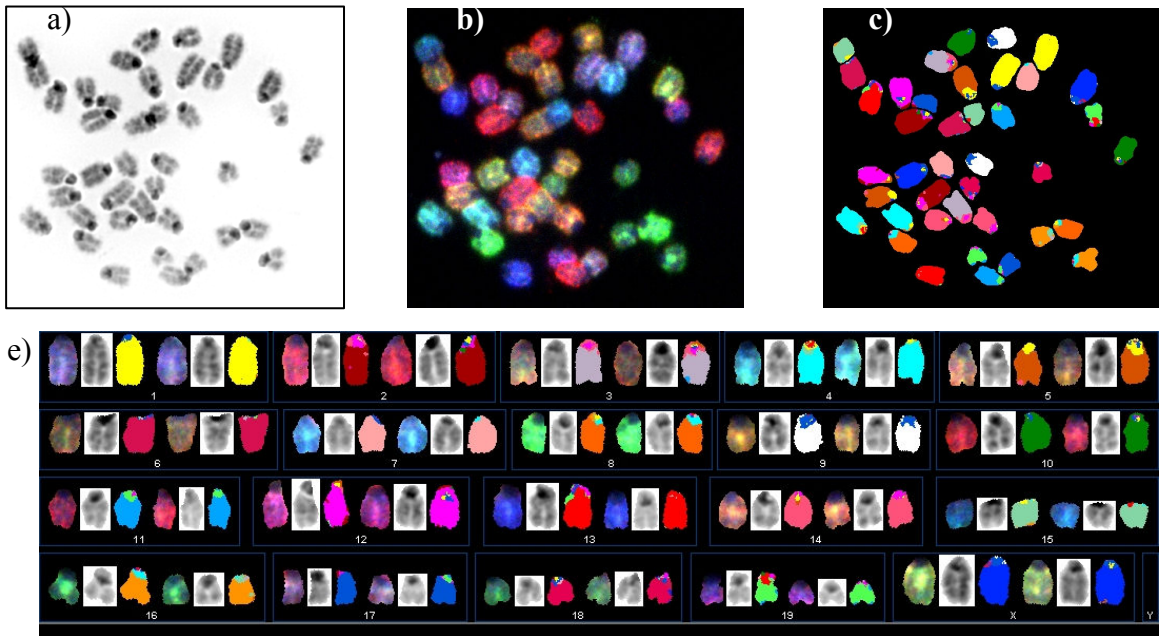


Figure 7. Spectral karyotype summary of mouse C3.13. Part a) schematically depicts karyotypes of LPS-induced splenocytes, where green blocks represent chromosome gain (trisomy or polysomy), and red blocks represent chromosome loss (monosomy or nullisomy). “None,” no aneuploidy; “Ch #,” number of chromosomes present in metaphase plate. Parts b), c), d), and e) represent inverted DAPI, spectral, classified, and karyotyped images of cell S35-04, respectively.

a) Summary of aneuploidy in near-diploid cells

Cell ID	1	2	3	4	5	6	7	8	9	10	11	12	13	14	15	16	17	18	19	X	None	Ch #	Notes		
S40-07																					X		40		
S40-08																						X		40	
S40-11																						X		40	
S40-12																						X		40	
S40-17																						X		40	
S40-18																						X		40	
S40-19																						X		40	
S40-20																						X		40	
S40-21																						X		40	
S40-22																						X		40	
S40-25																						X		40	
S40-26																						X		40	
S40-28																						X		40	
S40-02																								40	T(2;X), Ins(17;3)
S40-10	■	■																						39	
S40-30		■	■																					39	
S40-31								■	■									■	■					38	
S40-23	■	■	■																					41	extra ch 1 fragment
S40-24																								41	
S40-15						■	■								■	■								42	

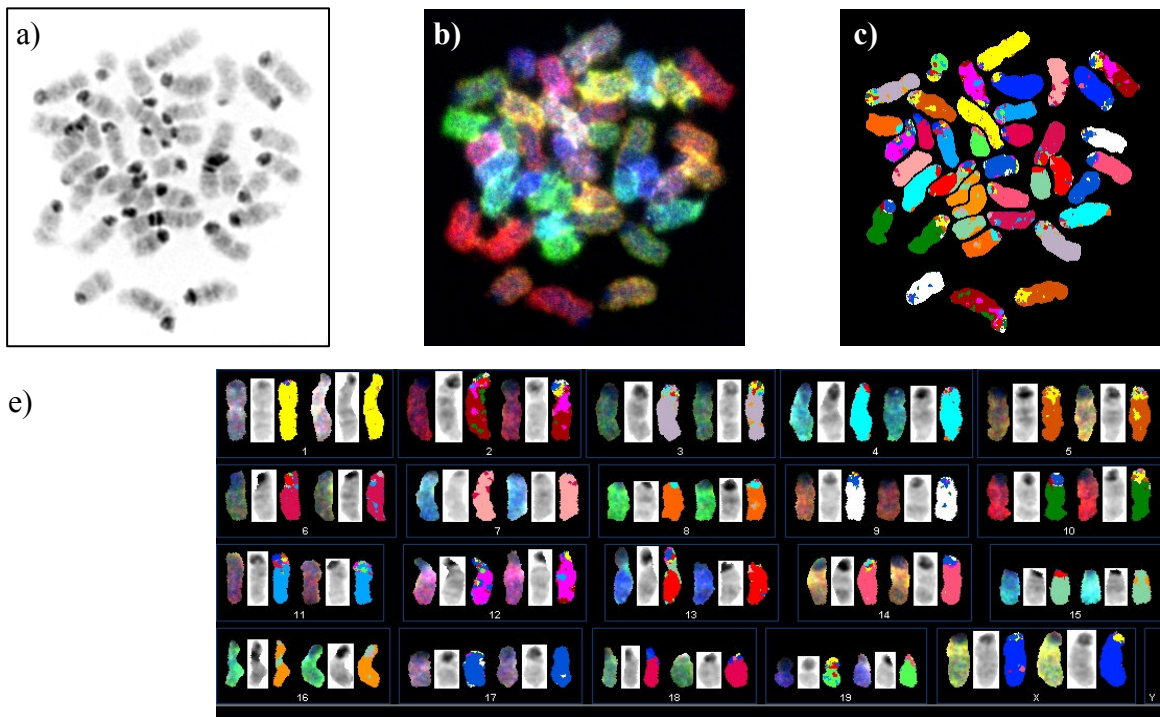


Figure 8. Spectral karyotype summary of mouse C5.17. Part a) schematically depicts karyotypes of LPS-induced splenocytes, where green blocks represent chromosome gain (trisomy or polysomy), and red blocks represent chromosome loss (monosomy or nullisomy). “None,” no aneuploidy; “Ch #,” number of chromosomes present in metaphase plate. Parts b), c), d), and e) represent inverted DAPI, spectral, classified, and karyotyped images of cell S40-17, respectively.

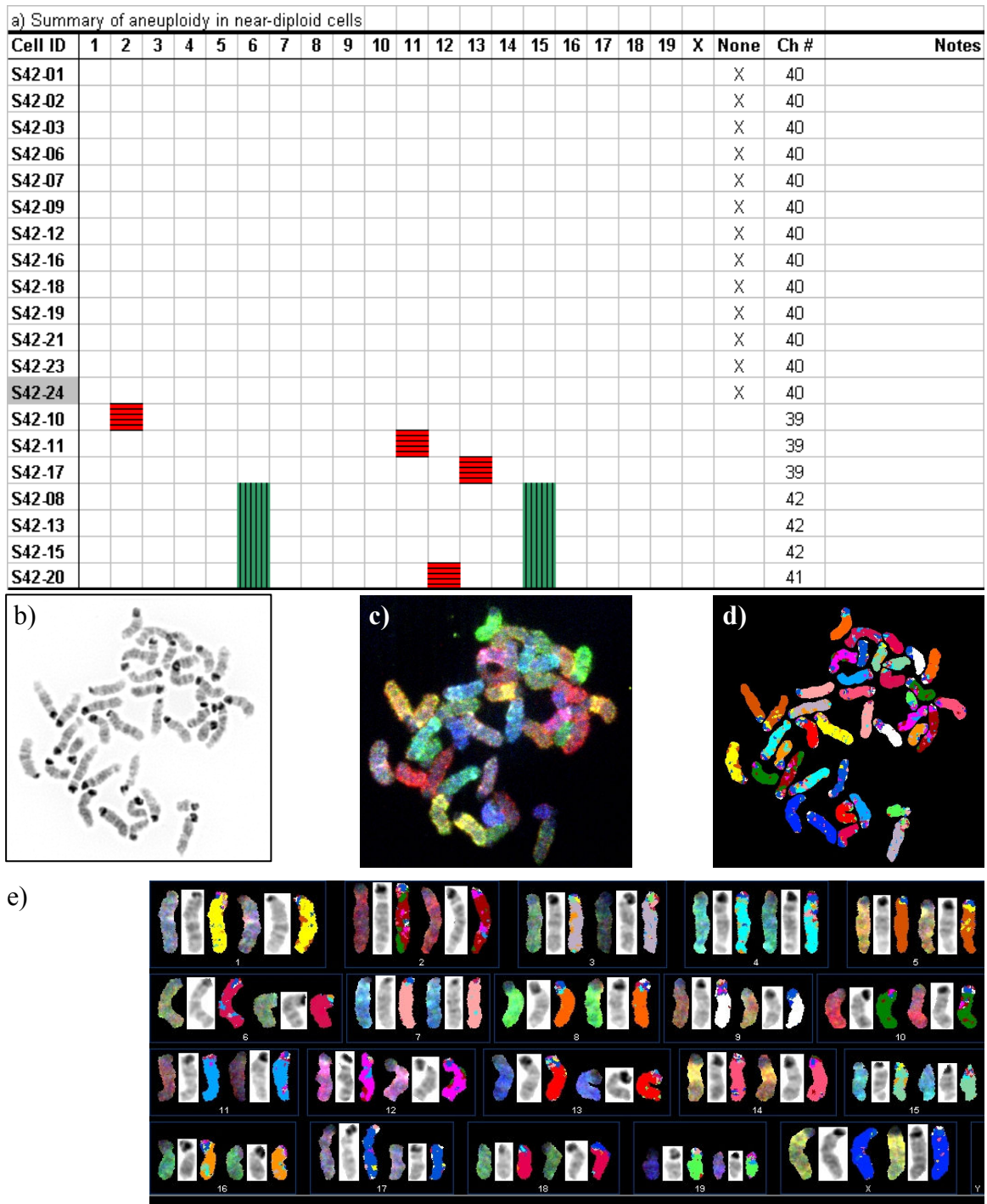


Figure 9. Spectral karyotype summary of mouse C3.16. Part a) schematically depicts karyotypes of LPS-induced splenocytes, where green blocks represent chromosome gain (trisomy or polysomy), and red blocks represent chromosome loss (monosomy or nullisomy). “None,” no aneuploidy; “Ch #,” number of chromosomes present in metaphase plate. Parts b), c), d), and e) represent inverted DAPI, spectral, classified, and karyotyped images of cell S42-24, respectively.

a) Summary of aneuploidy in near-diploid cells

Cell ID	1	2	3	4	5	6	7	8	9	10	11	12	13	14	15	16	17	18	19	X	None	Ch #	Notes		
S45-02																					X		40		
S45-06																						X		40	
S45-10																						X		40	
S45-13																						X		40	
S45-14																						X		40	
S45-15																						X		40	
S45-16																						X		40	
S45-17																						X		40	
S45-20																						X		40	
S45-21																						X		40	
S45-22																						X		40	
S45-23																						X		40	
S45-19																								39	
S45-18																								38	
S45-01																								42	
S45-05																								42	
S45-08																								42	
S45-09																								42	
S45-11																								42	
S45-12																								42	

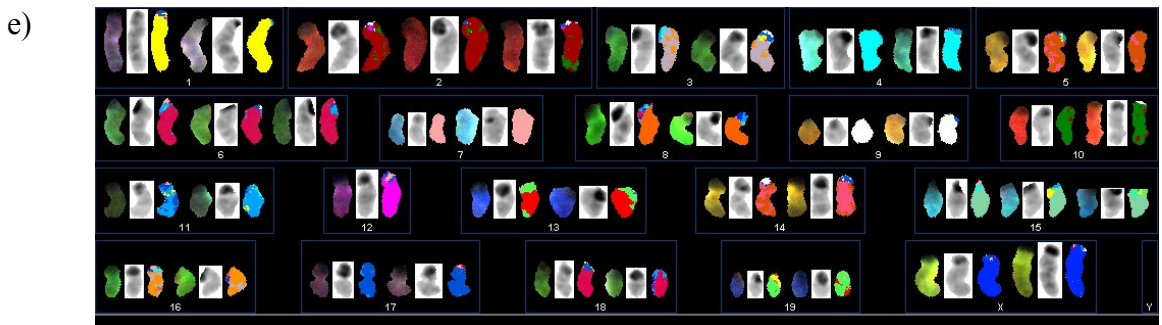
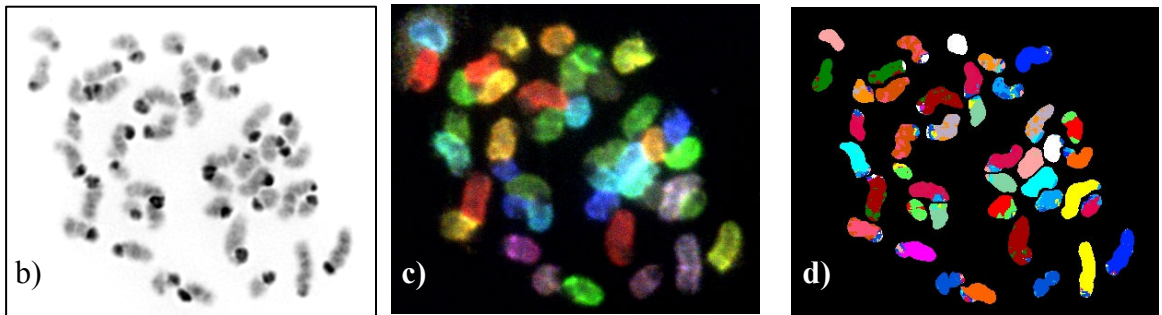


Figure 10. Spectral karyotype summary of mouse C3.17. Part a) schematically depicts karyotypes of LPS-induced splenocytes, where green blocks represent chromosome gain (trisomy or polysomy), and red blocks represent chromosome loss (monosomy or nullisomy). “None,” no aneuploidy; “Ch #,” number of chromosomes present in metaphase plate. Parts b), c), d), and e) represent inverted DAPI, spectral, classified, and karyotyped images of cell S45-09, respectively.

a) Summary of aneuploidy in near-diploid cells

Cell ID	1	2	3	4	5	6	7	8	9	10	11	12	13	14	15	16	17	18	19	X	None	Ch #	Notes		
S44.01																					X		40		
S44.02																						X		40	
S44.04																						X		40	
S44.10																						X		40	
S44.11																						X		40	
S44.12																						X		40	
S44.15									■	■														39	
S44.21																							■	39	
S44.16						■	■	■	■	■	■	■	■	■	■	■	■	■	■	■	■			42	
S44.14			■	■	■	■	■	■	■	■	■	■	■	■	■	■	■	■	■	■	■			40	
S44.19			■	■	■	■	■	■	■	■	■	■	■	■	■	■	■	■	■	■	■			39	
S44.03						■	■	■	■	■	■	■	■	■	■	■	■	■	■	■	■			43	
S44.05						■	■	■	■	■	■	■	■	■	■	■	■	■	■	■	■			43	
S44.06						■	■	■	■	■	■	■	■	■	■	■	■	■	■	■	■			43	
S44.07						■	■	■	■	■	■	■	■	■	■	■	■	■	■	■	■			43	
S44.08						■	■	■	■	■	■	■	■	■	■	■	■	■	■	■	■			43	
S44.09						■	■	■	■	■	■	■	■	■	■	■	■	■	■	■	■			43	
S44.13						■	■	■	■	■	■	■	■	■	■	■	■	■	■	■	■			43	
S44.18						■	■	■	■	■	■	■	■	■	■	■	■	■	■	■	■			43	
S44.20						■	■	■	■	■	■	■	■	■	■	■	■	■	■	■	■			43	

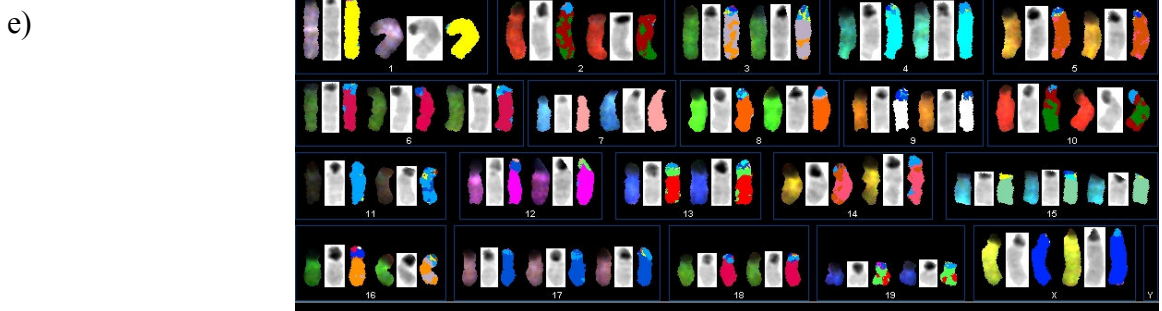
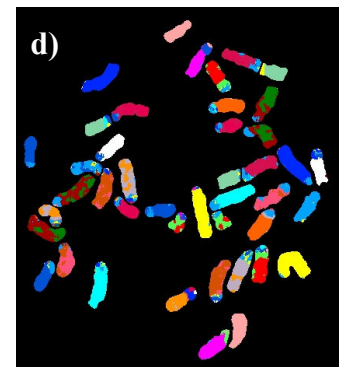
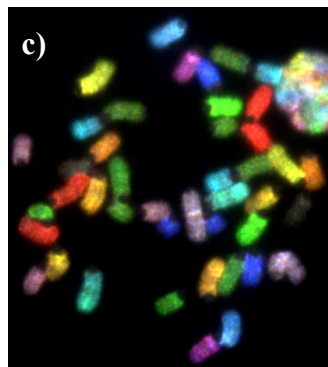
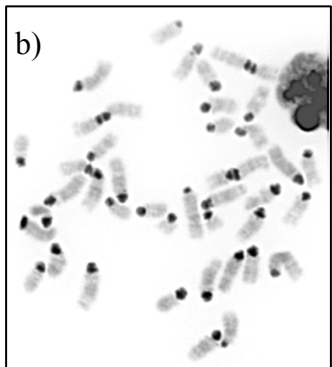


Figure 11. Spectral karyotype summary of mouse C1.17. Part a) schematically depicts karyotypes of LPS-induced splenocytes, where green blocks represent chromosome gain (trisomy or polysomy), and red blocks represent chromosome loss (monosomy or nullisomy). “None,” no aneuploidy; “Ch #,” number of chromosomes present in metaphase plate. Parts b), c), d), and e) represent inverted DAPI, spectral, classified, and karyotyped images of cell S44-18, respectively.

a) Summary of aneuploidy in near-diploid cells

Cell ID	1	2	3	4	5	6	7	8	9	10	11	12	13	14	15	16	17	18	19	X	None	Ch #	Notes		
S09-19																					X		40		
S09-24																								38	
S09-21	■		■							■														37	
S09-05											■	■	■	■	■	■	■	■	■	■	■			41	
S09-07											■	■	■	■	■	■	■	■	■	■	■			41	
S09-09											■	■	■	■	■	■	■	■	■	■	■			41	
S09-10											■	■	■	■	■	■	■	■	■	■	■			41	
S09-15											■	■	■	■	■	■	■	■	■	■	■			41	
S09-25											■	■	■	■	■	■	■	■	■	■	■			41	
S09-27											■	■	■	■	■	■	■	■	■	■	■			41	T(12;2)
S09-28											■	■	■	■	■	■	■	■	■	■	■			41	
S09-30											■	■	■	■	■	■	■	■	■	■	■			41	
S09-32											■	■	■	■	■	■	■	■	■	■	■			41	
S09-33											■	■	■	■	■	■	■	■	■	■	■			41	
S09-40											■	■	■	■	■	■	■	■	■	■	■			41	
S09-42											■	■	■	■	■	■	■	■	■	■	■			41	
S09-17											■	■	■	■	■	■	■	■	■	■	■			41	
S09-08											■	■	■	■	■	■	■	■	■	■	■			40	EEs
S09-38											■	■	■	■	■	■	■	■	■	■	■			40	
S09-23											■	■	■	■	■	■	■	■	■	■	■			42	
S09-34											■	■	■	■	■	■	■	■	■	■	■			39	
S09-35											■	■	■	■	■	■	■	■	■	■	■			39	
S09-18	■	■	■								■	■	■	■	■	■	■	■	■	■	■			37	

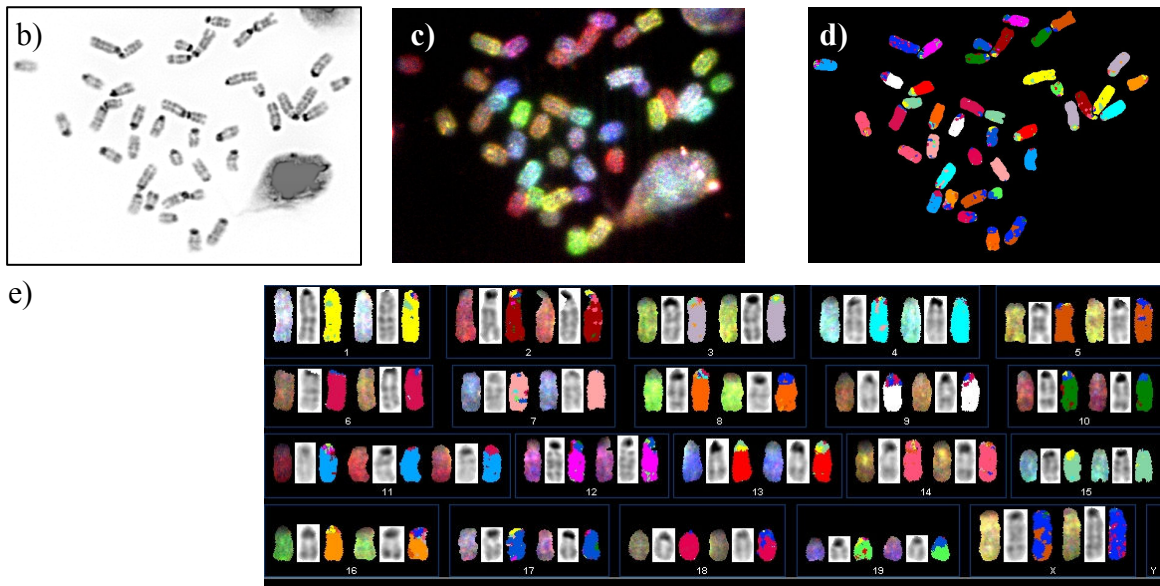


Figure 12. Spectral karyotype summary of mouse 3.14. Part a) schematically depicts karyotypes of pristane + ABL-MYC virus-induced tumour cells, where green blocks represent chromosome gain (trisomy or polysomy), and red blocks represent chromosome loss (monosomy or nullisomy). “None,” no aneuploidy; “Ch #,” number of chromosomes present in metaphase plate; “EEs,” extrachromosomal elements. Parts b), c), d), and e) represent inverted DAPI, spectral, classified, and karyotyped images of cell S09-32, respectively.

a) Summary of aneuploidy in near-diploid cells

Cell ID	1	2	3	4	5	6	7	8	9	10	11	12	13	14	15	16	17	18	19	X	None	Ch #	Notes	
S29-15																					X	40		
S05-08, 09									■										■				39	
S05-10, S01-36									■										■				38	
S05-01										■	■	■	■	■	■	■	■	■	■	■			41	rcp[T(2;12)]
S05-02										■	■	■	■	■	■	■	■	■	■	■			41	
S05-07										■	■	■	■	■	■	■	■	■	■	■			41	
S29-06										■	■	■	■	■	■	■	■	■	■	■			41	
S29-10										■	■	■	■	■	■	■	■	■	■	■			41	
S29-11										■	■	■	■	■	■	■	■	■	■	■			41	
S29-12										■	■	■	■	■	■	■	■	■	■	■			41	
S29-13										■	■	■	■	■	■	■	■	■	■	■			41	
S29-18										■	■	■	■	■	■	■	■	■	■	■			41	
S05-03										■	■	■	■	■	■	■	■	■	■	■			40	
S05-04										■	■	■	■	■	■	■	■	■	■	■			40	
S29-02										■	■	■	■	■	■	■	■	■	■	■			40	
S05-06				■	■				■	■	■	■	■	■	■	■	■	■	■	■			38	
S29-08				■	■				■	■	■	■	■	■	■	■	■	■	■	■			40	
S29-09										■	■	■	■	■	■	■	■	■	■	■			40	rcp[T(12;19)]
S01-37, 38										■	■	■	■	■	■	■	■	■	■	■			40	
S29-03										■	■	■	■	■	■	■	■	■	■	■			41	
S29-07			■	■					■	■	■	■	■	■	■	■	■	■	■	■			39	

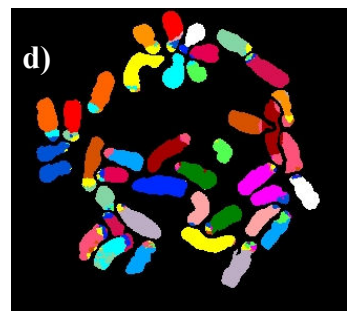
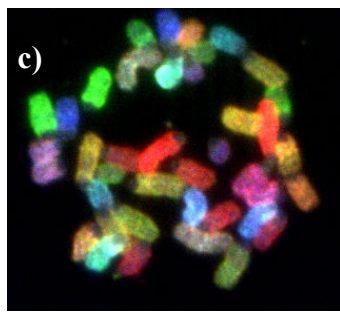
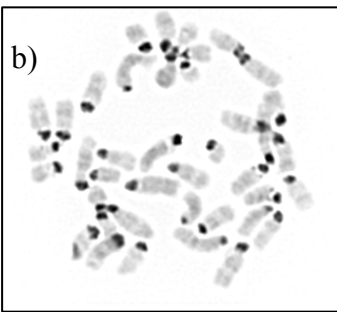
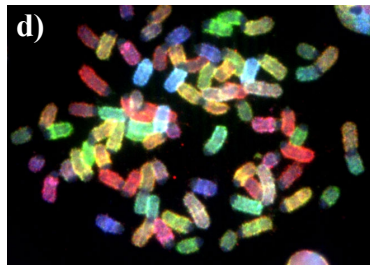
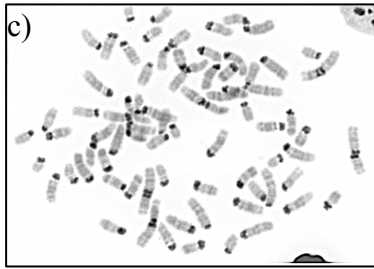


Figure 13. Spectral karyotype summary of mouse 2.7. Part a) schematically depicts karyotypes of pristane + ABL-MYC virus-induced tumour cells, where green blocks represent chromosome gain (trisomy or polysomy), and red blocks represent chromosome loss (monosomy or nullisomy). “None,” no aneuploidy; “Ch #,” number of chromosomes present in metaphase plate. Parts b), c), d), and e) represent inverted DAPI, spectral, classified, and karyotyped images of cell S29-08, respectively.

a) Summary of aneuploidy in near-diploid cells																									
Cell ID	1	2	3	4	5	6	7	8	9	10	11	12	13	14	15	16	17	18	19	X	None	Ch #	Notes		
S10-08																					X		40		
S18-09																						X		40	ch 14 separated
S18-17																						X		40	
S18-32																						X		40	EEs
S18-36														■	■									39	T(19;11)
S10-06											■	■	■	■	■	■	■	■	■	■				41	
S10-09											■	■	■	■	■	■	■	■	■	■				41	
S10-10											■	■	■	■	■	■	■	■	■	■				41	
S10-15											■	■	■	■	■	■	■	■	■	■				41	
S10-17											■	■	■	■	■	■	■	■	■	■				41	
S18-01											■	■	■	■	■	■	■	■	■	■				41	
S18-06											■	■	■	■	■	■	■	■	■	■				41	
S18-07											■	■	■	■	■	■	■	■	■	■				41	
S18-10											■	■	■	■	■	■	■	■	■	■				41	
S18-15											■	■	■	■	■	■	■	■	■	■				41	
S18-22											■	■	■	■	■	■	■	■	■	■				41	
S18-26											■	■	■	■	■	■	■	■	■	■				41	
S18-40											■	■	■	■	■	■	■	■	■	■				41	
S10-14											■	■	■	■	■	■	■	■	■	■				40	
S18-02		■	■								■	■	■	■	■	■	■	■	■	■				40	
S18-33											■	■	■	■	■	■	■	■	■	■				39	
S10-07											■	■	■	■	■	■	■	■	■	■				39	M
S19-21	■	■									■	■	■	■	■	■	■	■	■	■				38	
S18-29				■	■						■	■	■	■	■	■	■	■	■	■				38	
S18-03	■	■									■	■	■	■	■	■	■	■	■	■				37	
S18-25											■	■	■	■	■	■	■	■	■	■				42	
S18-23				■	■						■	■	■	■	■	■	■	■	■	■				38	
S18-14											■	■	■	■	■	■	■	■	■	■				41	T(19;11)
S18-24											■	■	■	■	■	■	■	■	■	■				41	T(19;11)
S18-37											■	■	■	■	■	■	■	■	■	■				41	T(19;11)
S18-39											■	■	■	■	■	■	■	■	■	■				41	T(19;11)

b) Summary of aneuploidy in near-tetraploid cells																								
Cell ID	1	2	3	4	5	6	7	8	9	10	11	12	13	14	15	16	17	18	19	X	None	Ch #	Notes	
S18-27, 28									■	■	■	■	■	■							■		77	M
S18-20			■	■					■	■	■	■	■	■									79	
S18-19											■	■	■	■	■	■	■	■	■	■			82	
S18-30, 31					■	■					■	■	■	■	■	■	■	■	■	■			80	
S18-35											■	■	■	■	■	■	■	■	■	■			82	M
S18-18		■	■						■	■	■	■	■	■			■	■	■	■			77	
S18-04	■	■	■	■	■	■	■	■	■	■	■	■	■	■	■	■	■	■	■	■	■	■	88	M
S18-13	■	■	■	■	■	■	■	■	■	■	■	■	■	■	■	■	■	■	■	■	■	■	123	sextaploid

Figure 14. Spectral karyotype summary of mouse 3.15. Parts a) and b) schematically depict karyotypes of pristane + ABL-MYC virus-induced near-diploid and near-tetraploid tumour cells, respectively, where green blocks represent chromosome gain (trisomy or polysomy), and red blocks represent chromosome loss (monosomy or nullisomy). “None,” no aneuploidy; “Ch #,” number of chromosomes present in metaphase plate; “EEs,” extrachromosomal elements. Parts c), d), e), and f) (see next page) represent inverted DAPI, spectral, classified, and karyotyped images of cell S18-19, respectively.



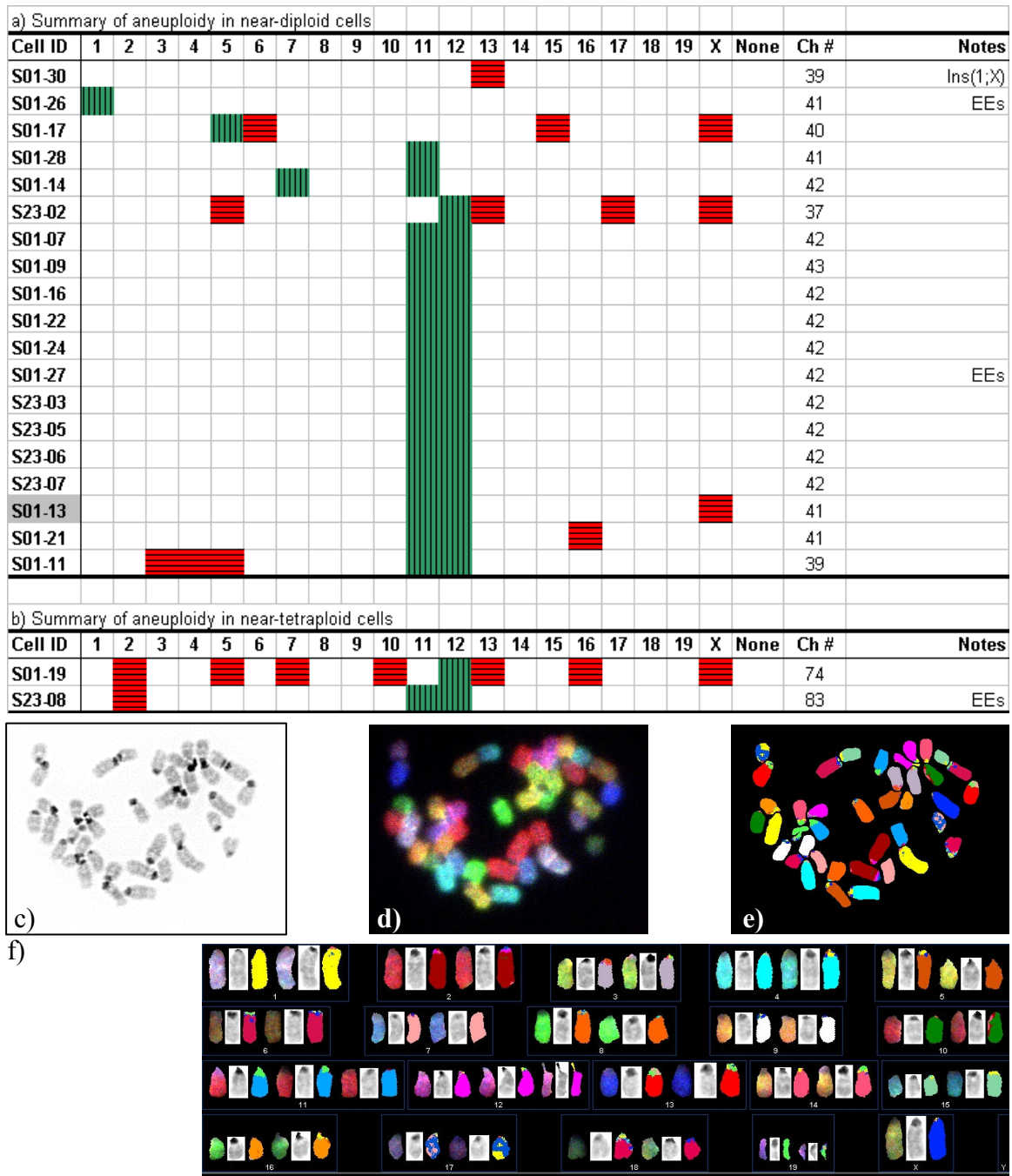


Figure 15. Spectral karyotype summary of mouse 1.12. Parts a) and b) schematically depict karyotypes of pristane + ABL-MYC virus-induced near-diploid and near-tetraploid tumour cells, respectively, where green blocks represent chromosome gain (trisomy or polysomy), and red horizontal blocks represent chromosome loss (monosomy or nullisomy). “None,” no aneuploidy; “Ch #,” number of chromosomes present in metaphase plate; “EEs,” extrachromosomal elements. Parts c), d), e), and f) represent inverted DAPI, spectral, classified, and karyotyped images of cell S01-13, respectively.

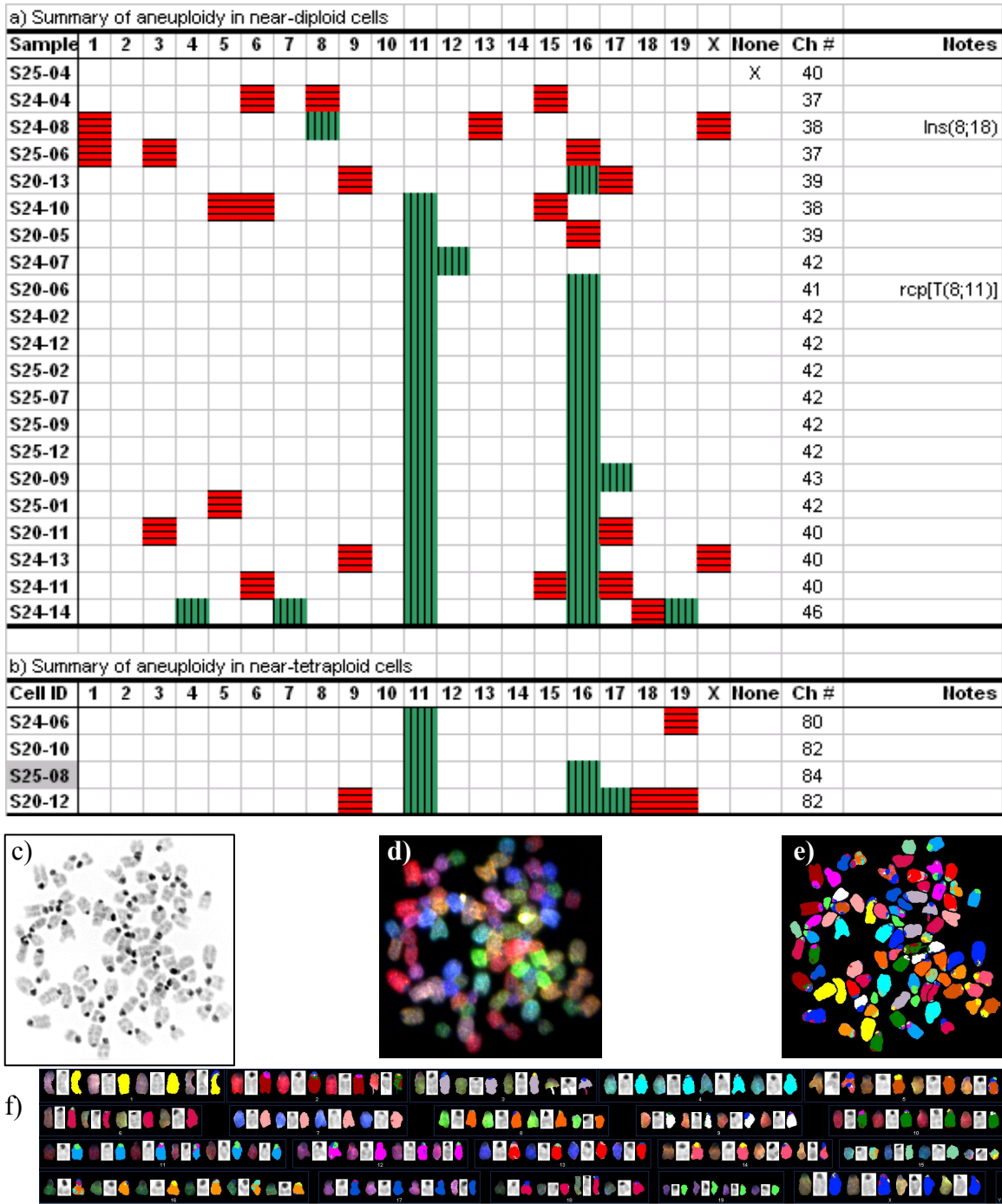


Figure 16. Spectral karyotype summary of mouse 2.14. Parts a) and b) schematically depict karyotypes of pristane + ABL-MYC virus-induced near-diploid and near-tetraploid tumour cells, respectively, where green blocks represent chromosome gain (trisomy or polysomy), and red blocks represent chromosome loss (monosomy or nullisomy). “None,” no aneuploidy; “Ch #,” number of chromosomes present in metaphase plate. Parts c), d), e), and f) represent inverted DAPI, spectral, classified, and karyotyped images of cell S25-08, respectively.

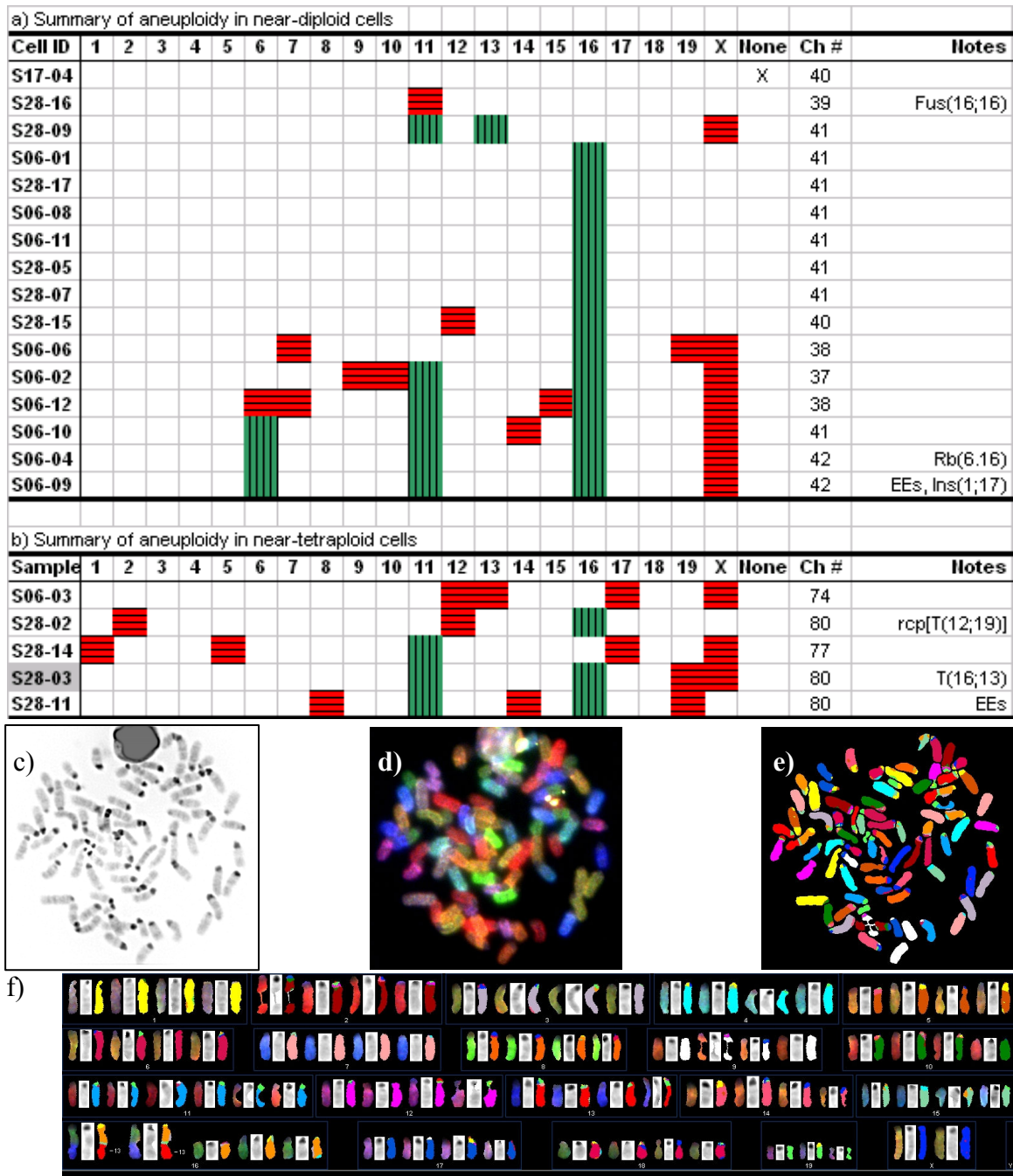


Figure 17. Spectral karyotype summary of mouse 1.11. Parts a) and b) schematically depict karyotypes of pristane + ABL-MYC virus-induced near-diploid and near-tetraploid tumour cells, respectively, where green blocks represent chromosome gain (trisomy or polysomy), and red blocks represent chromosome loss (monosomy or nullisomy). “None,” no aneuploidy; “Ch #,” number of chromosomes present in metaphase plate; “EEs,” extrachromosomal elements. Parts c), d), e), and f) represent inverted DAPI, spectral, classified, and karyotyped images of cell S28-03, respectively.

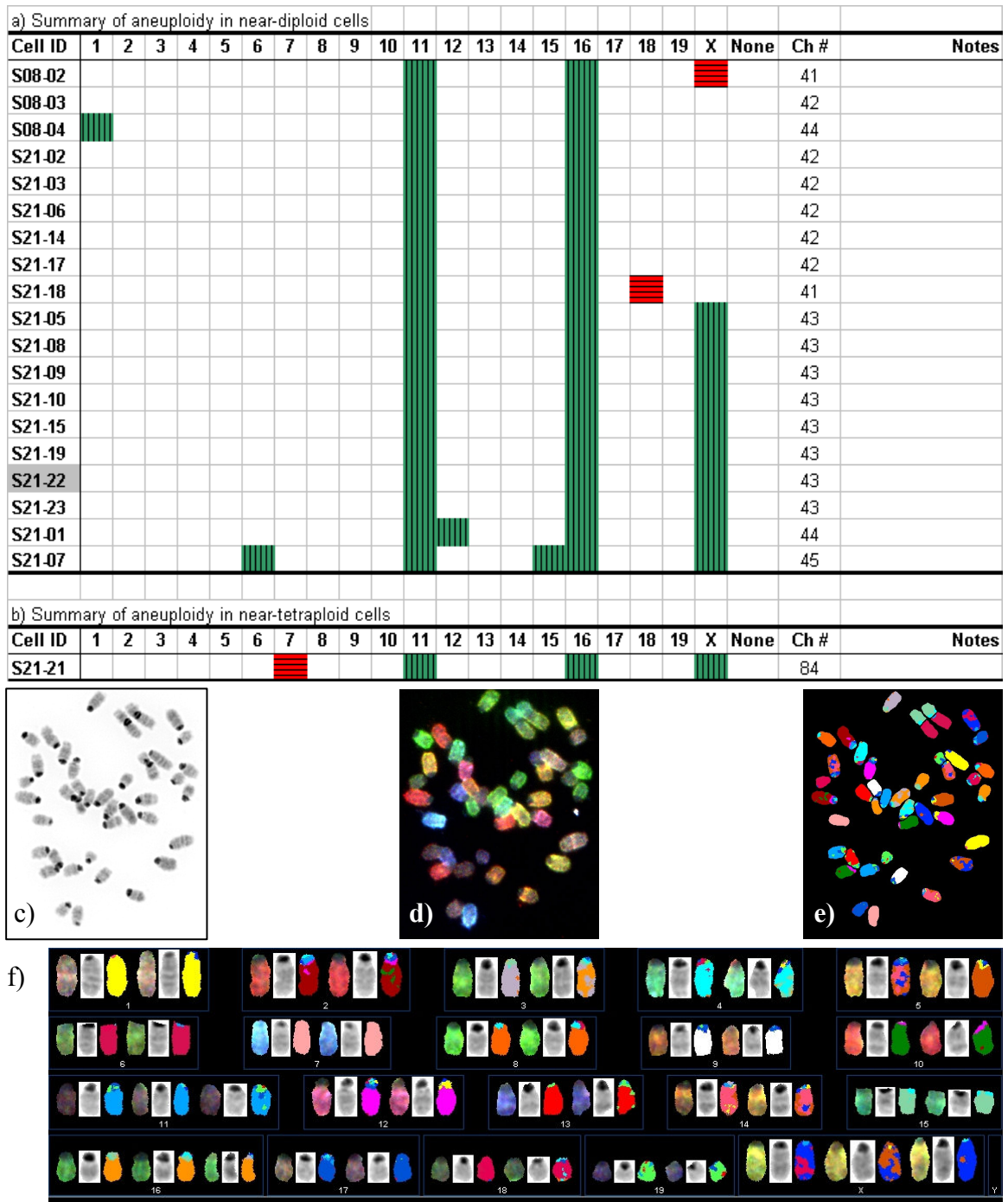


Figure 18. Spectral karyotype summary of mouse 1.13. Parts a) and b) schematically depict karyotypes of pristane + ABL-MYC virus-induced near-diploid and near-tetraploid tumour cells, respectively, where green blocks represent chromosome gain (trisomy or polysomy), and red blocks represent chromosome loss (monosomy or nullisomy). “None,” no aneuploidy; “Ch #,” number of chromosomes present in metaphase plate. Parts c), d), e), and f) represent inverted DAPI, spectral, classified, and karyotyped images of cell S21-22, respectively.

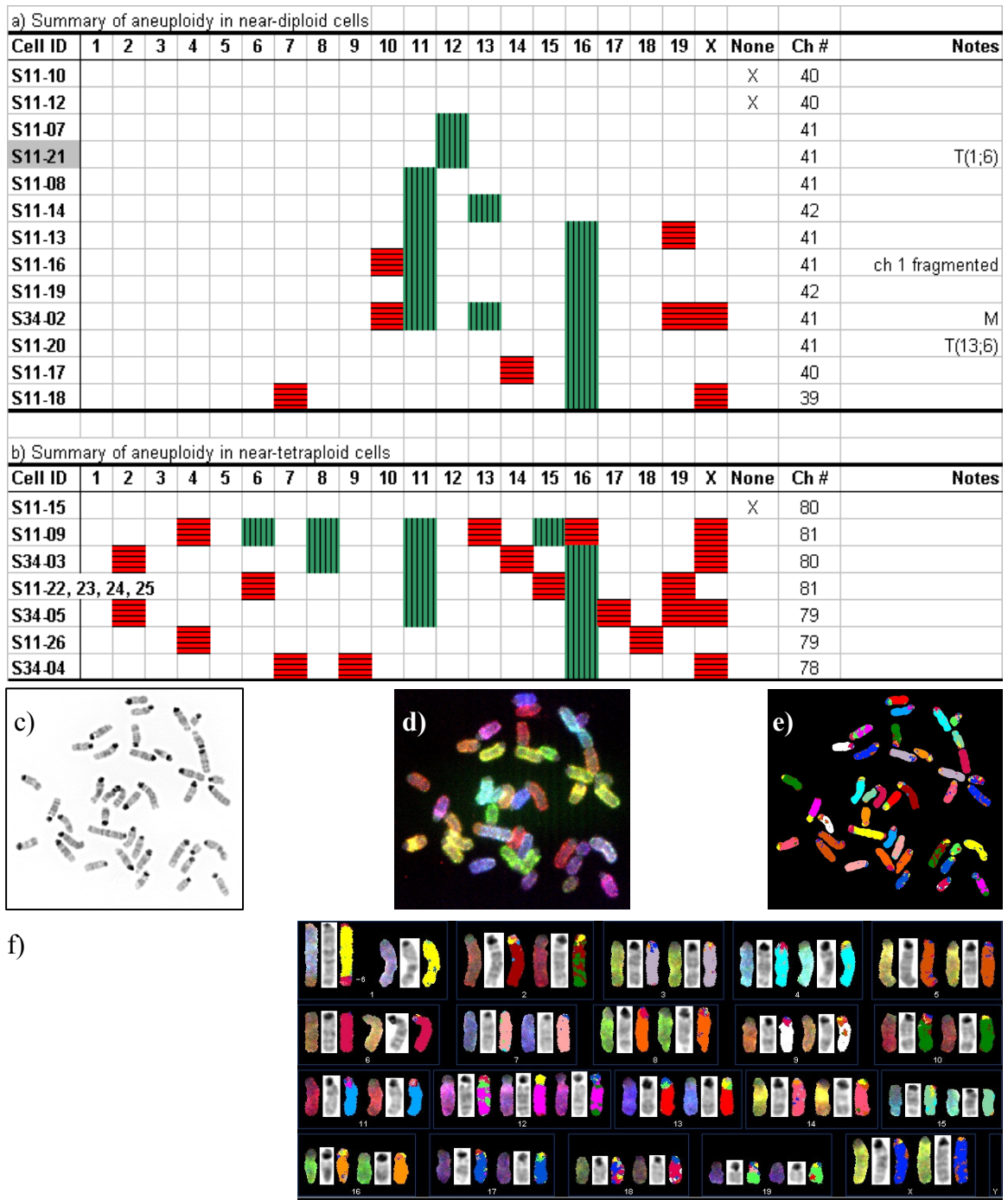
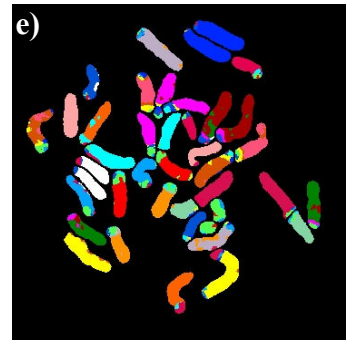
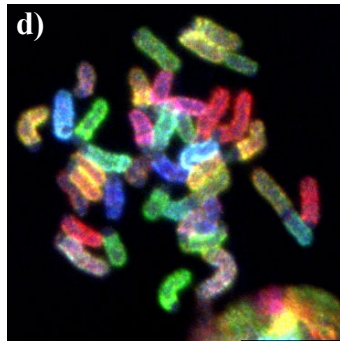


Figure 19. Spectral karyotype summary of mouse 4.15. Parts a) and b) schematically depict karyotypes of pristane + ABL-MYC virus-induced near-diploid and near-tetraploid tumour cells, respectively, where green blocks represent chromosome gain (trisomy or polysomy), and red blocks represent chromosome loss (monosomy or nullisomy). “None,” no aneuploidy; “Ch #,” number of chromosomes present in metaphase plate. Parts c), d), e), and f) represent inverted DAPI, spectral, classified, and karyotyped images of cell S11-21, respectively.

a) Summary of aneuploidy in near-diploid cells																									
Cell ID	1	2	3	4	5	6	7	8	9	10	11	12	13	14	15	16	17	18	19	X	None	Ch #	Notes		
S22-01																					X		40		
S22-08																						X		40	
S22-13																						X		40	
S22-05		■	■																					39	EEs
S22-09				■	■																			39	
S22-03												■	■	■										38	
S22-14																					■	■	■	39	
S22-15																						X		40	T(1;6)
S22-25																						X		40	T(1;6)
S22-32																					■	■	■	39	T(1;6)
S22-16												■	■	■	■	■	■							41	T(1;6)
S22-35												■	■	■	■	■	■							41	T(1;6)
S22-24												■	■	■	■	■	■				■	■	■	40	T(1;6)
S22-04																								41	
S22-07																								41	
S22-18																								41	
S22-22																								41	
S22-23																								41	T(13;6)
S22-30																								41	
S22-34																								41	
S22-10									■	■														40	
S22-21												■	■								■	■	■	40	
S22-31												■	■											42	
S22-29																								43	
S22-33																								43	
S22-26		■	■	■	■	■	■	■	■	■	■	■	■	■	■	■	■				■	■	■	48	T(1;6)

b) Summary of aneuploidy in near-tetraploid cells																								
Cell ID	1	2	3	4	5	6	7	8	9	10	11	12	13	14	15	16	17	18	19	X	None	Ch #	Notes	
S22-17	■	■	■			■					■	■	■	■	■	■				■			80	

Figure 20. Spectral karyotype summary of mouse 4.13. Parts a) and b) schematically depict karyotypes of pristane + ABL-MYC virus-induced near-diploid and near-tetraploid tumour cells, respectively, where green blocks represent chromosome gain (trisomy or polysomy), and red blocks represent chromosome loss (monosomy or nullisomy). “None,” no aneuploidy; “Ch #,” number of chromosomes present in metaphase plate; “EEs,” extrachromosomal elements. Parts c), d), e), and f) (see next page) represent inverted DAPI, spectral, classified, and karyotyped images of cell S22-35, respectively.



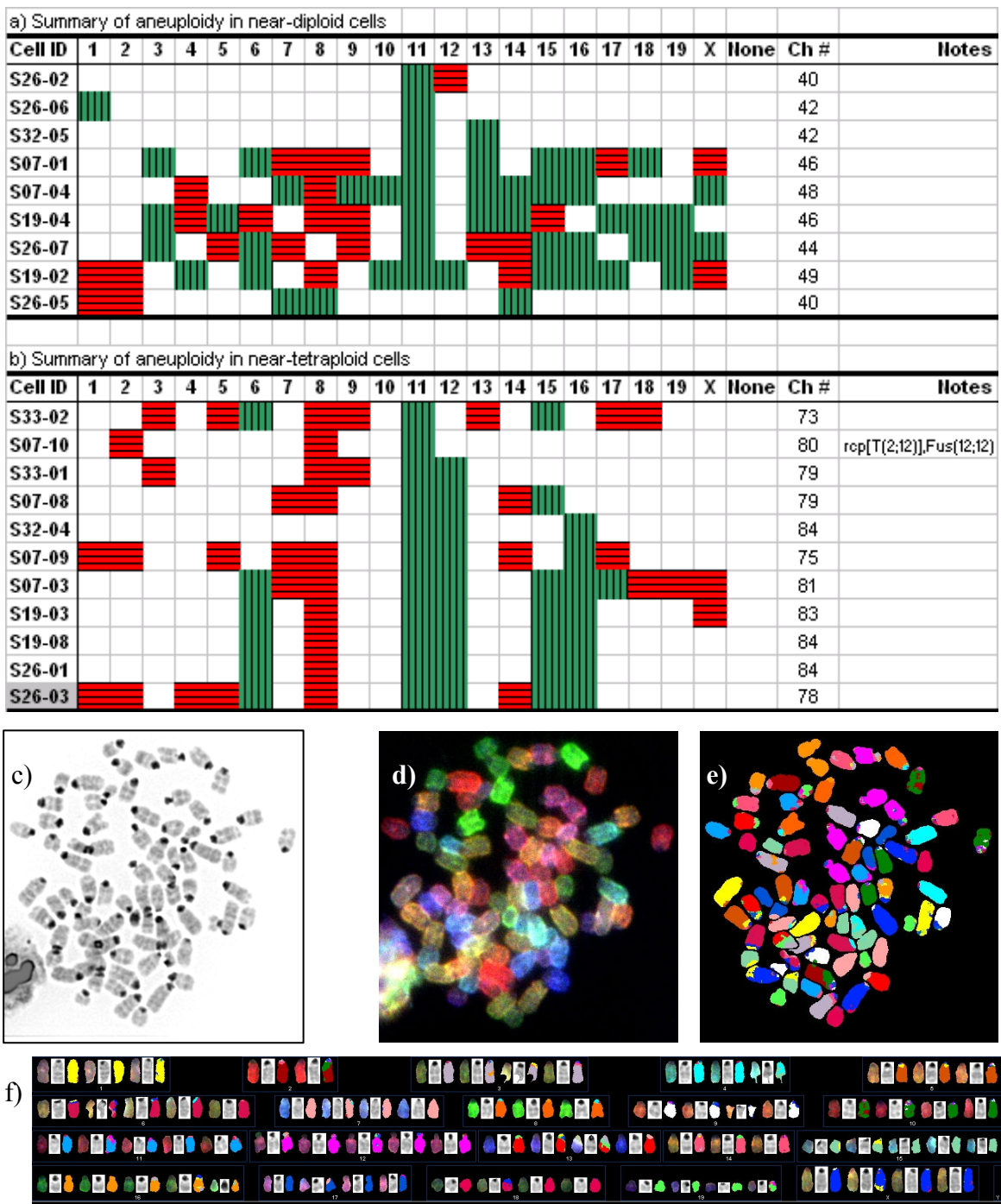


Figure 21. Spectral karyotype summary of mouse 1.14. Parts a) and b) schematically depict karyotypes of pristane + ABL-MYC virus-induced near-diploid and near-tetraploid tumour cells, respectively, where green blocks represent chromosome gain (trisomy or polysomy), and red blocks represent chromosome loss (monosomy or nullisomy). “None,” no aneuploidy; “Ch #,” number of chromosomes present in metaphase plate. Parts c), d), e), and f) represent inverted DAPI, spectral, classified, and karyotyped images of cell S26-03, respectively.

4. DISCUSSION

4.0 Effectiveness of pristane-treated mice as a control group

This study has confirmed the previously reported presence of trisomy 11 in pristane + ABL-MYC virus-induced plasmacytomas (Wiener *et al*, 1995), and has identified several new nonrandom cytogenetic mutations that also occur during plasmacytoma development. Mice injected only with pristane acted as a control group, allowing for separation of the effects of ABL-MYC virus infection from the widely established ability of pristane to act as a plasmacytomagenic agent and to produce tumours with *Myc*-activating translocations. However, control mice did not present the expected outcome of tumour cells bearing the T(12;15) or T(6;15) mutations, since plasmacytoma development was not observed.

Therefore, this study was unable to conclude that the addition of ABL-MYC virus to the induction protocol of pristane-treated BALB/cRb6.15 mice can potentiate a switch in the cytogenetic etiology of plasmacytoma. Contrary to this proposed dichotomy, it is possible that trisomy 11 and the other mutations identified in this study may be common to more than pristane + ABL-MYC virus-induced plasmacytomas, and that *Myc*-activating translocations may constitute only a partial account of the cytogenetic mutations present. However, only few studies provide evidence to support such a hypothesis, where tumour cells with a nonrandom presentation of trisomy 11 were produced upon treatment with pristane + A-MuLV (Ohno *et al*, 1984) or pristane + ABL-MYC virus (this study, and Wiener *et al*, 1995). Since the observance of this mutation has thus far been mainly limited to *v-abl*-containing retroviral induction methods, it is therefore quite possible that these mutations are correspondingly limited in incidence.

The failure of control mice to develop plasmacytoma can be best explained by the low dose of pristane used for treatment. The common induction regimen is three i.p. injections of pristane performed one to two months apart, where each injection is typically 0.3 ml (Mai and Wiener, 2002; and Silva *et al*, 2005) or 0.5 ml (Potter *et al*, 1997; and Bliskovsky *et al*, 2003). Two injections of 0.5 ml pristane have also induced plasmacytoma (Zhang *et al*, 2001). The trend among the various induction protocols using pristane invariably is the use of multiple injections, as well as total injected volumes in excess of the 0.3 ml used in the current study. Potter and Wax (1983) studied the effect of varied dose regimens on plasmacytomagenesis, and found that plasmacytoma induction efficiency positively correlated with volume of pristane injected, as well as number of injections. The study found that a single 0.05 ml dose was not effective, but did not present data between this exceedingly small single dose and a plasmacytoma-inducing single dose of 1.0 ml, and therefore did not define a minimal effective volume. Data from the current study suggest that a single 0.3 ml i.p. injection of pristane is not sufficient to induce plasmacytoma in BALB/cRb6.15 mice. Since the susceptibility of BALB/cAn mice (congenic to the BALB/cRb6.15 strain, but without the Robertsonian fusions joining both chromosomes 6 and 15) to pristane-induced plasmacytoma was found to decrease over a breeding period of eight years (Potter *et al*, 1994), it is also possible that a similar rise in resistance has affected the BALB/cRb6.15 strain, likely due to increased breeding in specific pathogen-free conditions (Byrd *et al*, 1991). Future studies comparing pristane treatment with the additional effects of ABL-MYC virus, where plasmacytoma development is desired in both groups, may achieve greater success using a larger pristane dose, such as 1.0 ml.

4.1 Nonrandom chromosome loss and random aneuploidy

Of the cytogenetic mutations observed, there were infrequent examples of nonrandom chromosome losses observed in control splenocytes and tumour cells. While loss of chromosome 7 in tumour cells was found to be statistically significant in comparison to control splenocytes, these results provide only weak evidence of nonrandom mutation, as the mutation occurred as infrequently as the loss of many other chromosomes. In contrast, a clearly nonrandom profile for chromosome loss in tumour cells was found for the X chromosome, where it contributed as a secondary mutation event in two of ten mice. However, it is difficult to assess the importance of X chromosome ploidy in plasmacytomagenesis, especially as it was also found amplified (as a secondary mutation event) in one mouse. In humans, loss of an X chromosome has been observed in females with childhood acute lymphoblastic leukemia (Riesch *et al*, 2001), while loss of the inactive X chromosome coupled with gain of the active X chromosome has been observed in breast cancer (Sirchia *et al*, 2005). Likewise, the seemingly conflicting results between tumour samples of the present study may possibly represent loss of one (active/inactive) X chromosome, or an alternative gain of the other chromosome, thereby similarly affecting chromosome imbalance. While loss of the inactivated X chromosome would theoretically have a minor effect, loss of the active X chromosome could have a major effect on gene expression and tumour physiology, and thus would be less likely to occur. Because only a minority of tumours in this study present ploidy changes of the X chromosome, the significance of this observation is unclear without further examination. A potential role for X chromosome inactivation and ploidy changes in ABL-MYC virus-induced murine plasmacytoma could be studied by

RNA fluorescent *in situ* hybridization (FISH) to detect *Xist* RNA binding to the inactivated X chromosome (indicating if the active or inactive X chromosome is amplified or deleted) (Brown *et al*, 1992; McCarrey and Dilworth, 1992), which would address the preliminary and unclear results of this study regarding X chromosome ploidy and its role in tumour development.

It is also difficult to determine the significance of random chromosome loss observed in both control splenocytes and tumour cells, acting as a background of aneuploidy contrasting with nonrandom chromosome gain. Tumour cells clearly showed a higher proportion of random chromosome loss than control splenocytes, and therefore reflect a higher degree of karyotypic instability. However, since the gain of random chromosomes within tumour samples occurred less frequently and in similar proportions to control splenocytes, it appears that random aneuploidy is predominated in BALB/cRb6.15 mice by chromosome loss. Since this study was limited to assessing karyotypes of B cells and their derivatives (plasmacytoma cells), it would be more accurate to conclude that this feature of aneuploidy may be only specific to these cells. A complimentary study might compare the proportions of chromosome gain and loss across other tumours, cell types, and mouse strains.

4.2 Nonrandom translocation and chromosome gain

In contrast to the uncertain significance of random chromosome loss and aneuploidy in tumour cells, the gain of chromosomes 11 and 16 was prominent and clearly associated with the tumour phenotype. While trisomy 11 has previously been described in pristane + ABL-MYC virus-induced plasmacytomas (Wiener *et al*, 1995), the other nonrandom karyotypic mutations identified in this study are novel findings. Since trisomies 11 and

16 were often found together in the same cell, these mutations together might confer distinct tumorigenic properties, since otherwise there would be no selective pressure to maintain both mutations in the tumour cell population. However, in the tumour samples from mice 3.15 and 4.13, either trisomy 11 or trisomy 16 was the single nonrandom karyotypic aberration found in a major proportion of cells, respectively. While both samples contained a minority of cells with other nonrandom aberrations, the principle aberration, trisomy 11 or trisomy 16, was also frequently the only karyotypic aberration of an individual cell. The tumour sample from mouse 3.14 shares this property of tumour growth without combination of trisomy 11 and trisomy 16, but indicates further that a single karyotypic aberration may underlie the growth of the complete tumour, since trisomy 11 was detected in this sample as the only nonrandom karyotypic aberration. Therefore, the amplification of both chromosomes together is clearly not necessary for tumour growth, even though it is a frequent occurrence. Because there was only one instance, in mouse 1.12, from which trisomies 11 and 16 were not detected together in the same tumour sample, it is clear that these trisomies are very important for plasmacytomagenesis using the pristane + ABL-MYC virus induction technique.

Trisomy 12 was also identified as a nonrandom karyotypic mutation, although less frequently than trisomies 11 or 16, and almost always in combination with another mutation. Since trisomy 12 was almost always observed in tandem with another pre-existing nonrandom karyotypic mutation, it may occur as a late mutation event or as an additional mutation that allows for increased tumour growth. This mutation was unique in that, as well as being present along with the primary mutation of trisomy 11, it also occurred with T(1;6), where a segment of chromosome 6 DNA was translocated to the q-

terminal region of chromosome 1. Although high resolution banding was not performed to identify which region was translocated, it was clear that this was not a reciprocal translocation event, as the Rb(6.15) chromosome appeared intact, without discernable material missing from the chromosome 6 region. Therefore, trisomy 12 was frequently found with partial trisomy of chromosome 6. Since seven of the eight detected cells harboring T(1;6) were only trisomic for chromosome 12, these results suggest that T(1;6) could act as a mutation analogous to trisomy 11, where trisomy 12 can occur in combination with either mutation.

Continued studies would ideally expand upon this hypothesis by identifying what region of chromosome 6 is translocated, and if any genes from the translocation-carrying chromosome are deregulated as a result. It is possible that the phenotype of T(1;6) is similar to that of trisomy 11, where the same biochemical or regulatory pathway is affected. A study currently underway in this laboratory aims to identify which region of chromosome 11 is necessarily amplified in pristane + ABL-MYC virus-induced plasmacytomagenesis, using T38H mice that harbor a reciprocal translocation between the X-chromosome and chromosome 11. Wiener *et al* (1995) have tentatively localized the region critical for amplification to band 11E, at the q-terminus of chromosome 11. The ongoing study with the T38H mice could confirm this result, and possibly narrow the region of interest further.

The absence of ABL-MYC tumour-associated karyotypic mutations in control mice suggests that either these mutations occur as a result of virus infection, or that there is no growth or survival advantage to cells carrying such mutations without the concomitant high expression of *v-abl* and *Myc* in the same cell. This second alternative could also

signify that ABL-MYC virus infection is not sufficient for transformation, but that a pre-existing mutation, such as trisomy 11, trisomy 16, or T(1;6), is also necessary. Such a hypothesis is supported by the fact that there are few metaphase plates from the ascites samples that do not contain one of these mutations. Also, as ascites also contains non-tumour lymphoid cells including lymphocytes, neutrophils, and macrophages, it is highly possible that metaphase plates without these karyotypic aberrations are not from tumour cells, but instead from proliferating lymphocytes or macrophages in response to the presence of tumour or oil granuloma.

While identifying tumour-specific mutations was expected in this study, the frequent gain of the Rb(6.15) chromosome in control splenocytes was unexpected, but was detected in six of seven samples. Statistical analysis did not link this mutation to the presence or absence of plasmacytoma development, since the difference in mutation frequency was not statistically significant between the two experimental groups. However, it is possible that trisomy of the Rb(6.15) chromosome is linked to oil granuloma development, which occurs within 30 days after a single i.p. injection of pristane (Potter *et al*, 1997), thereby acting as a tumour-promoting mutation. To evaluate this possibility, it would be important to compare data from this study with karyotypes from LPS-induced splenocytes of age-matched BALB/cRb(6.15) mice that have not received pristane treatment, which could determine if amplification of this chromosome was dependent upon i.p. pristane injection, and the resulting formation of oil granuloma. By determining the karyotypes of mice treated with pristane + ABL-MYC virus, it would be possible to evaluate the role of trisomy Rb(6.15) in rapidly developing plasmacytomas, which could more strongly associate a tumour-promoting effect. It

would be also beneficial to ascertain whether or not this mutation is present in pristane-induced plasmacytomas, although to date this has not been reported. However, there is some precedence for gain of Rb(6.15); trisomy 15 occurs spontaneously in aged mice, and may act as a factor for tumour development (Wiener *et al*, 1978).

This possible importance of trisomy Rb(6.15) also corresponds with the high prominence of *Myc*, present on both mouse chromosome 15, and the Rb(6.15) chromosome, in plasmacytomagenesis, and could lead to a growth advantage in splenocytes with this mutation (and other B cells/progenitors of plasmacytoma), explaining its frequent detection in tissue samples from apparently healthy mice of this study. However, the two pristane-treated mice that developed solid tumours (mice C2.16 and C1.15) yielded LPS-induced splenocytes with the lowest levels of aneuploidy, including trisomy Rb(6.15). These data indicate that trisomy Rb(6.15): (i) may not correlate with development of solid tumour formation in pristane-treated mice, but (ii) provides a selective growth advantage to B-lineage cells in a chronic inflammatory environment, and (iii) occurs in younger mice—as mice treated with pristane + ABL-MYC virus were all euthanized by approximately four months of age, with four of 10 samples presenting this mutation—as well as aged mice (e.g. in those treated with pristane, euthanized by approximately 17 months of age).

4.3 Additional mutations

In addition to the various nonrandom karyotypic mutations being evaluated on the basis of age, or of being present either alone or in combinations, there was also an added level of complexity across the samples of control splenocytes and tumour cells. Samples analyzed from each group presented a spectrum of karyotypic complexity ranging from

low to high levels of mutation (compare mice 3.14 and 1.14). Since differences in survival or pathology between mice could not be linked to this variability, it appears that the nonrandom plasmacytomagenic mutations characterized in this study do not determine the aggressiveness of tumour progression.

Also, frequent tetraploidy observed in tumour cells was not found in control splenocytes. While this difference in frequency was statistically significant and thus clearly correlated with tumour growth, the effect of this mutation is difficult to assess, since gene dosage is maintained. Tetraploidy was determined to be a secondary or tertiary mutation event in seven of ten tumour samples, indicating that this phenotype may experience positive selective pressure as a source for oncogenic mutations, while also acting sign of c-Myc-induced genomic instability leading to tumour initiation and progression (Prochownik and Li, 2007). It is possible that the observed tetraploidy may be a manifestation of a more general loss of control over genomic maintenance during cell division, such as impairment of centrosome function, chromosome segregation, and cytokinesis. A study on cytokinesis inhibition by Uetake and Sluder (2004), describing a lack of growth arrest during the G1 phase of newly-formed tetraploid cells, provides a possible explanation for the presence of tetraploidy; somatic cells may not contain a mechanism such as apoptosis to counteract this mutation, indicating that tetraploidy may not confer a significant danger or tumourigenic potential to the organism. However, the present study makes a clear correlation between tumour growth and tetraploidy, and therefore may alternatively indicate that it does play a significant role in models of oncogenesis such as murine plasmacytoma. Further, Li *et al* (2007) provide a specific link between c-Myc and tetraploidy, with expression of Gp1b α being upregulated by c-

Myc, and mediating both induction and maintenance of tetraploidy in immortalized and primary cell cultures. Since c-Myc is also overexpressed in pristine + ABL-MYC virus-induced tumours, it is possible that the observed tetraploidy is also due to Gp1b α overexpression.

It is also important to consider the variety of other nonrandom karyotypic mutations observed, mostly present as translocations in pristane + ABL-MYC virus-induced tumours. A tumour from one mouse (3.15) contained a cell subpopulation with T(11;19), where only a small amount of chromosome 11 material was translocated, approaching the limit of detection by spectral karyotyping. Pursuing these results with confirmatory mBAND or FISH using chromosome 11 paint (Benedek *et al*, 2004) could further evaluate this mutation as a possible nonrandom event. Since T(11;19) was detected in only one plasmacytoma sample, there is currently insufficient evidence to imply a significant role in the karyotypic etiology of this tumour. However, the variety of other chromosome translocations, fusions, insertions, and formation of extrachromosomal elements identify an underlying presence of chromosome instability that was not matched in control splenocytes. There were two instances of chromosome translocation in control splenocytes—rcp[T(12;14)] and T(2;X), in mice C2.16 and C5.17, respectively—indicating that numerical and structural aberrations are both present before tumour formation is anatomically evident. In this way, these mutations may indicate how an underlying rate of stochastic chromosome instability may result, at some point, in the generation of a mutation conferring growth potential to a precursor of the plasmacytoma cell.

4.4 Mutations in the context of other neoplasias

It is particularly interesting that trisomies 11, 12 and 16, and T(1;6) are each occurring in tumour cells that already overexpress *Myc*, due to expression from the integrated ABL-MYC virus (Largaespada *et al*, 1992), and therefore suggesting a requirement for additional changes in gene expression beyond the widely established importance of *Myc*. In pristane-induced plasmacytomas with the *Myc/Ig* translocation, it is possible that there are additional mutations either equal or analogous to the nonrandom karyotypic mutations described in the present study. McNeil *et al* (2005) have identified two plasmacytomas developed from IL-6 transgenic mice without characteristic *Myc/Ig* translocations, where one tumour showed evidence of chromosome 16 amplification. While the study did not thoroughly evaluate changes in chromosome ploidy, it does suggest that trisomy 16 may carry importance beyond pristane + ABL-MYC virus-induced plasmacytomas. The current study is the first to provide a full karyotypic profile of murine plasmacytomas (where karyotypes of individual cells among a tumour cell population is presented), and it would be advantageous for similar studies to be performed using other models of murine plasmacytomagenesis, in a search for similar and unique mutations across the variety of mouse models and induction methods.

There has been one study that illustrates this advantage; Coleman *et al* (2000) present a systematic analysis of a series of plasmacytomas induced by peritoneal injection of silicone or pristane, where 10 to 20 cells of each tumour were analyzed for cytogenetic mutations by SKY. Although karyotypes of individual tumour cells were not presented, the authors observed T(12;15) and T(15;6) as primary cytogenetic alterations, while secondary cytogenetic alterations included non-reciprocal translocations and partial

deletions of chromosome 5, as well as whole or partial addition of chromosome 1. These data were interpreted as possibly linking secondary karyotypic mutations occurring in murine plasmacytoma with mutations in human multiple myeloma, although further studies identifying any specific, analogous genetic events would still be required. Such results correspond with those of the present study, where there is a cytogenetic progression of accumulated mutations that can be observed in individual primary tumours, in addition to *Myc* activation that occurs with ABL-MYC virus infection and that is analogous to *Myc/Ig* translocation. While the *Myc/Ig* translocation has historically been a focus of study, isolating additional mutations shared by distinct tumours will provide a more encompassing understanding of murine plasmacytoma initiation and progression, and hopefully also extend to human carcinogenesis, including multiple myeloma and Burkitt's lymphoma.

Indicating a possibility for a new relation of murine plasmacytoma to human disease, chromosome 16, the second most frequently-affected chromosome for nonrandom karyotypic mutation in this study, carries significant homology with human chromosome 21, which is trisomic in Down syndrome. Children with Down syndrome have an increased incidence of developing acute lymphoblastic leukemia, acute myeloid leukemia, and acute megakaryoblastic leukemia (reviewed by Hitzler and Zipursky, 2005). The critical region of chromosome 21 for development of Down syndrome, 21q22, shares homology with mouse chromosome 16. It is conceivable that trisomy 16 in murine plasmacytoma may play a similar role to trisomy 21 in development of childhood leukemia. Since trisomy 16 has not previously been identified as a nonrandom event in murine plasmacytoma, it is important to note that pristine + ABL-MYC virus treatment

has not been extensively studied for its influence on cytogenetic events leading to plasmacytoma. While a study by Wiener *et al* (1995) detected trisomy 16 using this induction method, it was not identified as a nonrandom mutation, and its frequency within and among tumours was not shown. Therefore, it is possible that trisomy 16 may have occurred as a nonrandom event in previous studies of murine plasmacytoma, but was not detected.

IL-6 signaling, important for multiple myeloma and plasmacytoma cell growth and survival, also shows links to mutations observed in this study. Chromosome 11, most frequently affected by nonrandom mutation in this study, contains genes important to IL-6 signaling and plasmacytoma growth such as *Stat3* (Iankov *et al*, 2004), and *Prkca* (Romanova *et al*, 1996), which may confer increased neoplastic potential to cells if overexpressed due to trisomy 11. *Stat3* encodes STAT3, an activator of Myc signaling, and is activated in various cancers (reviewed by Calo *et al*, 2003), while *Prkca* encodes protein kinase C- α , an activator of various oncogenes, and is also important for many cancers through its various effects on cell growth and survival (reviewed by Michie and Nakagawa, 2005).

It would be interesting to assess the efficiency of ABL-MYC virus-induced plasmacytoma induction in mice lacking, for example, functional *Stat3* or *Prkca*, along with the karyotypic mutation profile of any developing plasmacytomas. To date, ABL-MYC virus has been consistently used to induce plasmacytomas with high efficiency, and identifying loci on chromosomes 11, 12, and 16 that are critical for ABL-MYC virus-induced plasmacytomagenesis may also translate to an importance of these loci for other cancers.

5. Conclusions

This study identifies trisomies 11 and 16 as frequent, nonrandom karyotypic mutations important for pristane + ABL-MYC virus-induced plasmacytomagenesis, where each may act as primary and initiating mutation events for tumour development. Also, trisomy 12 occurs less frequently in formation of this tumour, and possibly as a later or secondary event, in combination with another primary mutation such as trisomy 11, 16, or alternatively, T(1;6). The various combinations of these mutations observed within and among plasmacytomas suggest that there are several analogous and redundant steps towards karyotypic progression of plasmacytoma.

6. REFERENCES

Adams JM, AW Harris, CA Pinkert, LM Corcoran, WS Alexander, S Cory, RD Palmiter, RL Brinster. 1985. The c-myc oncogene driven by immunoglobulin enhancers induces lymphoid malignancy in transgenic mice. *Nature* 318:533-538.

Adams JM, S Gerondakis, E Webb, LM Corcoran, S Cory. 1983. Cellular myc oncogene is altered by chromosome translocation to an immunoglobulin locus in murine plasmacytomas and is rearranged similarly in human Burkitt lymphomas. *Proc Natl Acad Sci USA* 80:1982-1986.

Anisimov VN. 2003. The relationship between aging and carcinogenesis: a critical appraisal. *Crit Rev Oncol Hematol* 45:277-304.

Axelson H, CK Panda, S Silva, H Sugiyama, F Wiener, G Klein, J Sumegi. 1991. A new variant 15;16 translocation in mouse plasmacytoma leads to the juxtaposition of c-myc and immunoglobulin lamda. *Oncogene* 6:2263-2270.

Bakkus MH, C Heirman, I Van Riet, B Van Camp, K Thielemans. 1992. Evidence that multiple myeloma heavy chain VDJ genes contain somatic mutations but show no intraclonal variation. *Blood* 80:2326-2335.

Barille S, R Bataille, M Amiot. 2000. The role of interleukin-6 and interleukin-6/interleukin-6-receptor-alpha complex in the pathogenesis of multiple myeloma. Eur Cytokine Network 11:546-551.

Benedek K, I Chudoba, G Klein, F Wiener, S Mai. 2004. Rearrangements of the telomeric region of mouse chromosome 11 in Pre-B ABL/MYC cells revealed by mBANDing, spectral karyotyping, and fluorescence *in-situ* hybridization with a subtelomeric probe. Chromosome Res 12:777-785.

Bernard O, S Cory, S Gerondakis, E Webb, JM Adams. 1983. Sequence of the murine and human cellular myc oncogenes and two modes of myc transcription resulting from chromosome translocation in B lymphoid tumours. EMBO J 2:2375-2383.

Bliskovski V, ES Ramsay, J Scott, W DuBois, WSS Zhang, X Qian, DR Lowry, BA Mock. 2003. *Frap*, FKBP12 rapamycin-associated protein, is a candidate gene for the plasmacytoma resistance locus *Pctr2* and can act as a tumor suppressor gene. Proc Natl Acad Sci USA 100:14982-14987.

Brown CJ, BD Hendrich, JL Rupert, RG Lafreniere, Y Xing, J Lawrence, HF Willard. 1992. The human *XIST* gene: analysis of a 17 kb inactive X-specific RNA that contains several conserved repeats and is highly localized within the nucleus. Cell 71:527-542.

Byrd LG, AH MacDonald, LG Gold, M Potter. 1991. Specific pathogen-free BALB/cAn mice are refractory to plasmacytoma induction by pristane. *J Immunol* 147:3632-3637.

Calo V, Migliavacca, V Bazan, M Macaluso, M Buscemi, N Gebbia, A Russo. 2003. STAT proteins: from normal control of cellular events to tumorigenesis. *J Cell Physiol* 197:157-168.

Coene ED, V Schelfhout, RA Winkler, AM Schelfhout, N Van Roy, M Grooteclaes, F Speleman, CR De Potter. 1997. Amplification units and translocation at chromosome 17q and c-erbB-2 overexpression in the pathogenesis of breast cancer. *Virchows Arch* 430:365-372.

Coleman AE, T Ried, S Janz. 2000. Chromosomes 1 and 5 harbor plasmacytoma progressor genes in mice. *Genes Chromosomes Cancer* 29:70-74.

Cory S, M Graham, E Webb, L Corcoran, J Adams. 1985. Variant (6;15) translocations in murine plasmacytomas involve a chromosome 15 locus at least 72 kb from the *c-myc* oncogene. *EMBO J* 3:675-681.

Davis M, S Malcolm, TH Rabitts. 1984. Chromosome translocation can occur on either side of the *c-myc* oncogene in Burkitt's lymphoma cells. *Nature* 308:286-288.

Degrassi A, DM Hilbert, S Rudikoff, AO Anderson, M Potter, HG Coon. 1993. *In vitro* culture of primary plasmacytomas requires stromal cell feeder layers. Proc Natl Acad Sci USA 90:2060-2064.

Dunnick W, BE Shell, C Dery. 1983. DNA sequences near the site of reciprocal recombination between a *c-myc* oncogene and an immunoglobulin switch region. Proc Natl Acad Sci USA 80:7269-7273.

Fest T, V Mougey, V Dalstein, M Hagerty, D Milette, S Silva, S Mai. 2002. c-MYC overexpression in Ba/F3 cells simultaneously elicits genomic instability and apoptosis. Oncogene 21:2981-2990.

Fong KM, Y Kida, PV Zimmerman, M Ikenaga, PJ Smith. 1995. Loss of heterozygosity frequently affects chromosome 17q in non-small cell lung cancer. Cancer Res. 55:4268-4272.

Gadó K, S Silva, K Pálóczi, G Domján, A Falus. 2001. Mouse plasmacytoma: an experimental model of human multiple myeloma. Haematologica 86:227-236.

Gaillard JP, J Liautard, B Klein, J Brochier. 1997. Major role of the soluble interleukin-6/interleukin-6 receptor complex for the proliferation of interleukin-6-dependent human myeloma cell lines. Eur J Immunol 27:3332-3340.

Gao X, A Zackarek, A Salkowski, DJ Grignon, W Sakr, AT Porter, KV Honn. 1995. Loss of heterozygosity of the BRCA1 and other loci on chromosome 17q in human prostate cancer. *Cancer Res* 55:1002-1005.

Gartel AL, K Shchors. 2003. Mechanisms of c-myc-mediated transcriptional repression of growth arrest genes. *Exp Cell Res* 283:17-21.

Goff SP, E Gilboa, ON Witte, D Baltimore. 1980. Structure of the Abelson murine leukemia virus genome and the homologous cellular gene: studies with cloned viral DNA. *Cell* 22:777-785.

Hermans A, N Heisterkamp, M von Linden, S van Baal, D Meijer, D van der Plas, LM Wiedemann, J Groffen, D Bootsma, G Grosveld. 1987. Unique fusion of *bcr* and *c-abl* genes in Philadelphia chromosome positive acute lymphocytic leukemia. *Cell* 51:33-40.

Hilbert DM, M Kopf, BA Mock, G Kohler, S Rudikoff. 1995. Interleukin 6 is essential for in vivo development of B lineage neoplasms. *J Exp Med* 182:243-248.

Hitzler JK, A Zipursky. 2005. Origins of leukaemia in children with Down syndrome. *Nat Rev Cancer* 5:11-20.

Hollis GF, KF Mitchell, J Battey, H Potter, R Taub, GM Lenoir, P Leder. 1984. A variant translocation places the lamda immunoglobulin genes 3' to the c-myc oncogene in Burkitt's lymphoma. *Nature* 307:752-755.

Iankov I, G Atanasova, M Praskova, S Kalenderova, D Petrov, V Mitev, I Mitov. 2004. Bacterial lipopolysaccharide induces proliferation of IL-6-dependent plasmacytoma cells by MAPK pathway activation. *Immunobiol* 208:445-454.

Janeway CA, P Travers, M Walport, M Shlomchik. 2001. *Immunobiology: the immune system in health and disease* (5th ed.). New York: Garland Publishing.

Kawano M, T Hirano, T Matsuda, T Taga, Y Horii, K Iwato, H Asaoku, B Tang, O Tanabe, H Tanaka, A Kuramoto, T Kishimoto. 1988. Autocrine generation and requirement of BSF-2/IL-6 for human multiple myelomas. *Nature* 332:83-85.

Janz S, J Müller, J Shaughnessy, M Potter. 1993. Detection of recombinations between c-myc and immunoglobulin switch alpha in murine plasma cell tumors and preneoplastic lesions by polymerase chain reaction. *Proc Nat Acad Sci* 90:7361-7365.

Klein G. 1995. B-cell neoplasia in a developmental framework. *Int J Dev Biol* 39:713-718.

Kovalchuk AL, JS Kim, SS Park, AE Coleman, JM Ward, HC Morse III, T Kishimoto, M Potter, S Janz. 2002. IL-6 transgenic mouse model for extraosseous plasmacytoma. Proc Natl Acad Sci USA 99:1509-1514.

Kovalchuk AL, JS Kim, S Janz. 2003. *E μ /S μ* transposition into *Myc* is sometimes a precursor for T(12;15) translocation in mouse B cells. Oncogene 22:2842-2850.

Kyle RA, SV Rajkumar. 2003. Monoclonal gammopathies of undetermined significance: a review. Immunol Rev 194:112-139.

Largaespada DA, DA Kaehler, H Mishak, E Weissinger, M Potter, JF Mushinski, R Risser. 1992. A retrovirus that expresses *v-abl* and *c-myc* oncogenes rapidly induces plasmacytomas. Oncogene 7:811-819.

Largaespada DA, MW Jackson, NE Thompson, DA Kaehler, LG Byrd, JF Mushinski. 1996. The ABL-MYC retrovirus generates antigen-specific plasmacytomas by in vitro infection of activated B lymphocytes from spleen and other murine lymphoid organs. J Immunol Methods 197:85-95.

Lastowska M, YJ Chung, N Cheng Ching, M Haber, MD Norris, UR Kees, AD Pearson, MS Jackson. 2004. Regions syntenic to human 17q are gained in mouse and rat neuroblastoma. Genes Chromosomes Cancer 40:158-163.

Li Y, J Lu, EV Prochownik. 2007. c-Myc-mediated genomic instability proceeds via a megakaryocytic endomitosis pathway involving Gp1b α . Proc Natl Acad Sci USA 104:3490-3495.

Lowrey PL, JS Takahashi. 2004. Mammalian circadian biology: elucidating genome-wide levels of circadian organization. Annu Rev Genomics Hum Genet 5:407-441.

Mai S, JF Mushinski. 2003. c-Myc-induced genomic instability. J Environ Pathol Toxicol Oncol 22:179-199.

Mai S, F Wiener. 2002. The impact of *p53* loss on murine plasmacytoma development. Chromosome Res 10:239-251.

McCarrey JR, DD Dilworth. 1992. Expression of *Xist* in mouse germ cells correlates with X-chromosome inactivation. Nat Genet 2:200-203.

McNeil N, JS Kim, T Ried, S Janz. 2005. Extrasosseous IL-6 transgenic mouse plasmacytoma sometimes lacks *Myc*-activating chromosomal translocation. Genes Chromosomes Cancer 43:137-146.

Merwin RM, Algire GH. 1959. Induction of plasma cell neoplasms and fibrosarcomas in BALB/c mice carrying diffusion chambers. Proc Soc Exp Biol Med. 101:437-439.

Michie AM, R Nakagawa. 2005. The link between PKC α regulation and cellular transformation. *Immunol Lett* 96:155-162.

Müller JR, GM Jones, S Janz, M Potter. 1997. Migration of cells with immunoglobulin/*c-myc* recombinations in lymphoid tissues of mice. *Blood* 89:291-296.

Nowell PC, DA Hungerford. 1960. A minute chromosome in human chronic granulocytic leukemia. *Science* 132:1497-1501.

Ohno S, J Hayakawa, N Hashimoto, F Wiener. 1999. Murine plasmacytomas, carrier of the t(12;15) chromosomal translocation, develop from immature/mature B cells and not from differentiated plasma cells. *Carcinogenesis* 20:529-538.

Ohno S, M Babonitis, Wiener F, J Spira, G Klein, M Potter. 1979. Nonrandom chromosome changes involving the Ig gene-carrying chromosomes 12 and 6 in pristane-induced mouse plasmacytomas. *Cell* 18:1001-1007.

Ohno S, S Migita, F Wiener, M Babonitis, G Klein, FJ Mushinski, M Potter. 1984. Chromosomal translocation activating *myc* sequences and transduction of *v-abl* are critical events in the rapid induction of plasmacytomas by pristane and Abelson virus. *J Exp Med* 159:1762-1777.

Paulin FE, MJ West, NF Sullivan, RL Whitney, L Lyne, AE Willis. 1996. Aberrant translational control of the *c-myc* gene in multiple myeloma. *Oncogene* 13:505-513.

Potter M. 2003. Neoplastic development in plasma cells. *Immunol Rev* 194:177-195.

Potter M, RC MacCardle. 1964. Histology of developing plasma cell neoplasia induced by mineral oil in Balb/C mice. *J Natl Cancer Inst* 33:497-515.

Potter M, EB Mushinski, JS Wax, J Hartley, BA Mock. 1994. Identification of two genes on chromosome 4 that determine resistance to plasmacytoma induction in mice. *Cancer Res* 54:969-975.

Potter M, MD Sklar, WP Rowe. 1973. Rapid viral induction of plasmacytomas in pristane-primed BALB-c mice. *Science* 182:592-594.

Potter M, JS Wax. 1983. Peritoneal plasmacytomagenesis in mice: comparison of different pristane dose regimens. *J Natl Cancer Inst* 71:391-395.

Potter M, J Wax, GM Jones. 1997. Indomethacin is a potent inhibitor of pristane and plastic disc induced plasmacytomagenesis in a hypersusceptible BALB/c congenic strain. *Blood* 90:260-269.

Potter M, F Wiener. 1992. Plasmacytomagenesis in mice: model of neoplastic development dependent upon chromosomal translocations. *Carcinogenesis* 13:1681-1697.

Prochownik EV, Y Li. 2007. The ever expanding role of c-Myc in promoting genomic instability. *Cell Cycle* 6:1024-1029.

Radl J, C Van Arkel, CM Hopstaken, H HogenEsch. 1996. Ten-fold increased incidence of spontaneous multiple myeloma in long-term immunosuppressed aging C57BL/KaLwRij mice. *Clin Immunol Immunopathol* 79:155-162.

Riesch M, FK Niggli, K Leibundgut, U Caflisch, DR Betts. 2001. Loss of X chromosome in acute childhood lymphoblastic leukemia. *Cancer Genet Cytogenet* 125:27-29.

Romana SP, M Le Conait, R Berger. 1994. t(12;21): a new recurrent translocation in acute lymphoblastic leukemia. *Genes Chromosom Cancer* 9:186-191.

Romanova LY, IA Alexandrov, G Schwab, DM Hilbert, JF Mushinski, RP Nordan. 1996. Mechanism of apoptosis suppression by phorbol ester IL-6-starved murine plasmacytomas: role of PKC modulation and cell cycle. *Biochemistry* 35:9900-9906.

Rosenbaum H, AW Harris, ML Bath, J McNeall, E Webb, J M.Adams, S Cory. 1990. An E μ -v-*abl* transgene elicits plasmacytomas in concert with an activated *myc* gene. *EMBO* 9:897-905.

Rosenberg NE, DR Clark, ON Witte. 1980. Abelson murine leukemia virus mutants deficient in kinase activity and lymphoid cell transformation. *J Virol* 36:766-774.

Rowley JD. 1973. A new consistent chromosomal abnormality in chronic myelogenous leukemia identified by quinacrine fluorescence and Giemsa staining. *Nature* 243:290-293.

Saito H, J Inazawa, S Saito, Kasumi F, S Koi, S Sagae, R Kudo, J Saito, K Noda, Y Nakamura. 1993. Detailed deletion mapping of chromosome 17q in ovarian and breast cancers: 2-cM region on 17q21.3 often and commonly deleted in tumours. *Cancer Res* 53:3382-3385.

Selvanayagam P, M Blick, F Narni, P van Tuinen, DH Ledbetter, R Alexanian, GF Saunders, B Barlogie. 1988. Alteration and Abnormal Expression of the *c-myc* oncogene in human multiple myeloma. *Blood* 71;30-35.

Seidl S, H Kaufmann, J Drach. 2003. New insights into the pathophysiology of multiple myeloma. *Lancet Oncol* 4:557-564.

Shapiro-Shelef M, K Calame. 2004. Plasma cell differentiation and multiple myeloma. *Curr Opin Immunol* 16:226-234.

Silva S, AL Kovalchuk, JS Kim, G Klein, S Janz. 2003. *BCL2* accelerates inflammation-induced BALB/c plasmacytomas and promotes novel tumors with coexisting T(12;15) and T(6;15) translocations. *Cancer Res* 63:8656-8663.

Silva S, F Wiener, G Klein, S Janz. 2005. Location of *Myc*, *Igh*, and *Igk* on Robertsonian fusion chromosomes is inconsequential for *Myc* translocations and plasmacytoma development in mice, but Rb(6.15)-carrying tumors prefer *Igk-Myc* inversions over translocations. *Genes Chromosomes Cancer* 42:416-426.

Sirchia SM, L Ramoschelli, FR Grati, F Barbera, D Coradini, F Rossella, G Porta, E Lesma, A Ruggeri, P Radice, G Simoni, M Miozzi. 2005. Loss of the X chromosome and replication of the active X in BRCA1-defective and wild-type breast cancer cells. *Cancer Res* 65:2139-2146.

Siwarski D, U Müller, J Andersson, V Notario, F Melchers, A Rolink, K Huppi. 1997. Structure and expression of the c-Myc/Pvt 1 megagene locus. *Curr Top Microbiol Immunol* 224:67-72.

Smid V. Personal communication. Central Animal Care Services, University of Manitoba.

Stevenson FK, SS Sahota, CH Ottensmeier, D Zhu, F Forconi, TJ Hamblin. 2001. The occurrence and significance of V gene mutations in B cell-derived human malignancy. *Adv Cancer Res* 83:81-116.

Sugiyama H, S Silva, YS Wang, G Weber, M Babonitis, A Rosen, F Wiener, G Klein. 1990. Abelson murine leukemia virus transforms preneoplastic E μ -*myc* transgene-carrying cells of the B-lymphocyte lineage into plasmablastic tumors. *Int J Cancer* 46:845-852.

Taub R, I Kirsch, C Morton, G Lenoir, D Swan, S Tronick, S Aaronson, P Leder. 1982. Translocation of the *c-myc* gene into the immunoglobulin heavy chain locus in human Burkitt lymphoma and murine plasmacytoma cells. *Proc Natl Acad Sci USA* 79:7837-7841.

Thabard W, M Collette, R Bataille, M Amiot. 2001. Protein kinase C δ and η isozymes control the shedding of the interleukin 6 receptor α in myeloma cells. *Biochem J* 358:193-200.

Uetake Y, G Sluder. 2004. Cell cycle progression after cell cleavage failure: mammalian cells do not possess a "tetraploidy checkpoint." *J Cell Biol* 165:609-615.

Urashima M, A Ogata, D Chauhan, M Hatziyanni, MB Vidriales, DA Dederer, RL Schlossman, KC Anderson. 1996. Transforming growth factor-beta1: differential effects on multiple myeloma versus normal B cells. *Blood* 87:1928-1938.

Vanderkerken K, K Asosingh, P Croucher, B Van Camp. 2003. Multiple myeloma biology: lessons from the 5TMM models. *Immunol Rev* 194:196-206.

Varis A, M Wolf, O Monni, ML Vakkari, A Kokkola, C Moskaluk, H Frierson Jr, SM Powell, S Knuutila, A Kallioniemi, W El-Rifai. 2002. Targets of gene amplification and overexpression at 17q in gastric cancer. *Cancer Res* 62:2625-2629.

Weissinger EM, H Mischak, J Goodnight, WF Davidson, JF Mushinski. 1993. Addition of constitutive *c-myc* expression to Abelson murine leukemia virus changes the phenotype of cells transformed by the virus from pre-B-cell lymphomas to plasmacytomas. *Mol Cell Biol* 13:2578-2585.

Weissinger EM, H Mischak, DA Largaespada, DA Kaehler, T Mitchell, SJ Smith-Gill, R Risser, JF Mushinski. 1991. Induction of plasmacytomas secreting antigen-specific monoclonal antibodies with a retrovirus expressing *v-abl* and *c-myc*. *Proc Natl Acad Sci USA* 88:8735-8739.

Wiener F, A Coleman, BA Mock, M Potter. 1995. Nonrandom chromosomal change (Trisomy 11) in murine plasmacytomas induced by an ABL-MYC retrovirus. *Cancer Res* 55:1181-1188.

Wiener F, S Ohno, J Spira, N Haran-Ghera, G Klein. 1978. Cytogenetic mapping of the chromosome segment of chromosome 15 in murine T-cell leukaemia. *Nature* 275:658-660.

Zhang S, W DuBois, ES Ramsey, V Bliskovski, HC Morse III, L Taddesse-Heath, WC Vass, RA DePinho, B Mock. 2001. Efficiency alleles of the *Pctr1* modifier locus for plasmacytoma susceptibility. *Mol Cell Biol* 21:310-318.

Zhang S, ES Ramsay, BA Mock. 1998. *Cdkn2a*, the cyclin-dependent kinase inhibitor encoding p16^{INK4a} and p19^{ARF}, is a candidate for the plasmacytoma susceptibility locus, *Pctr1*. *Proc Natl Acad Sci USA* 95:2429-2434.

Zhang S, X Qian, C Redman, V Bliskovski, ES Ramsay, DR Lowry, BA Mock. 2003. p16^{INK4a} gene promoter variation and differential binding of a repressor, the ras-responsive zinc-finger transcription factor, RREB. *Oncogene* 22:2285-2295.